Response of isolated footing on a geogrid reinforced fill and undisturbed peat subgrade soil system

Accepted Manuscript – Not the final published version

Aykut Erol[1], Zulkuf Kaya[1]

Aykut Erol

(First Author)

Research Assistant (Dr.)

[1]Erciyes University, Department of Civil Engineering, Kayseri, Türkiye

aykuterol@erciyes.edu.tr

ORC ID: 0000-0003-3206-8133

Zulkuf Kaya

(Corresponding Author)

Professor

[1]Erciyes University, Department of Civil Engineering, Kayseri, Türkiye

zkaya@erciyes.edu.tr

ORC ID: 0000-0002-0180-7362

ACCEPTED MANUSCRIPT

This is the accepted version of the manuscript accepted for publication in Geotextiles and Geomembranes.

The final published version will be available via its DOI: https://doi.org/10.1016/j.geotexmem.2025.05.001

© 2025 Elsevier. This version is made available under the CC BY-NC-ND 4.0 license, in accordance with Elsevier's sharing policy.

Abstract

The geotechnical behavior of undisturbed peat subgrade within geogrid-reinforced foundation systems remains inadequately understood, despite its high compressibility and engineering complexities. This study conducts a systematic investigation into the bearing capacity and settlement characteristics of an isolated footing on geogrid-reinforced fill over undisturbed peat, utilizing laboratory-scale model tests. Unlike previous studies that rely on disturbed peat samples, this research preserves natural stratification and in-situ response mechanisms, providing a more accurate representation of reinforcement performance. The results demonstrate that geogrid reinforcement enhances bearing capacity by up to 149.7% and mitigates settlement by 79%, with optimal reinforcement efficiency achieved at h/B = 0.3. These findings underscore the critical role of geogrid embedment depth, fill thickness, and relative density in optimizing foundation stability. By integrating undisturbed peat in physical modeling, this study bridges the gap between controlled laboratory experiments and real-world geotechnical applications, providing a framework for optimizing geosynthetic reinforcement strategies in highly compressible subgrades and paving the way for more reliable foundation designs in challenging ground conditions.

Keywords: Geogrids, Model tests, Bearing capacity, Peat soil, Isolated footing

ACCEPTED MANUSCRIPT

Introduction

In the 21st century, the increasing scarcity of suitable land for construction has emerged as a significant challenge for geotechnical engineers. The growing demand for infrastructure, including buildings, railways, highways, and other critical structures, has made it increasingly necessary to build on weak or unstable soils. This trend has prompted engineers worldwide to explore and implement ground improvement techniques that are tailored to specific site conditions and project requirements. These methods aim to enhance the bearing capacity and mitigate settlement issues of weak soils, ensuring that construction activities can be carried out safely and effectively in areas previously considered unsuitable for development (Aminu et al., 2022; Apurva et al., 2022; Razali et al., 2013; Rikmann et al., 2021).

Peat soil is classified as a weak or soft soil type, posing significant engineering challenges for the construction of structures. Unlike non-organic soils, peat exhibits distinct behavioral characteristics that necessitate specialized consideration in geotechnical engineering. This soil is primarily composed of organic material, with over 75% of its content being organic matter, which significantly influences its physical properties. Even small amounts of organic substances in the soil can substantially alter its behavior, particularly affecting its shear strength and compressibility. Typically composed of fine particles such as silt or clay, organic soils are often categorized as organic silty or clayey soils.

Peat properties are primarily influenced by its botanical composition, fiber content, and degree of decomposition (Rezanezhad et al., 2016). The degree of decomposition, or humification, is commonly classified using the von Post scale, a 10-step system in which H1 represents minimally decomposed peat, whereas H10 indicates highly decomposed peat (Huat et al., 2011; Long, 2005). This classification is based on visual inspection and a squeezing test. The United States Department of Agriculture (USDA) simplifies the von Post scale into three categories: fibric (H1–H4), hemic (H5–H6), and sapric (H7–H10) (USDA, 1999). Fibric peat has over 66% fiber content, with distinguishable plant structures and minimal decomposition. Hemic peat exhibits a moderate level of decomposition with 33%–66% fiber content, while sapric peat, the most decomposed form, contains less than 33% fiber and appears dark brown to black due to its highly humified nature (ASTM, 1992). These classifications are crucial for assessing peat's geotechnical behavior, particularly in foundation engineering and soil reinforcement applications (Chmielewska, 2023).

The presence of fibrous organic material in these soils provides additional frictional resistance compared to soft silt or clay deposits, further complicating the behavior of peat in engineering applications (Hamed et al., 2020; Sulaiman et al., 2022). The low submerged unit weight of peat results in reduced effective self-weight stresses, stiffness, and undrained shear strength, which are essential factors in foundation design. These properties significantly influence the engineering behavior of peat under loading. Its low bearing capacity and high compressibility lead to substantial primary and secondary consolidation, resulting in excessive long-term settlement (Kaya and Erol, 2021; Peng et al., 2023). Laboratory tests indicate that peat typically exhibits low undrained shear strength, ranging between 5 and 20 kPa. In the referenced studies conducted in the same region, an undrained shear strength of 9.8

ACCEPTED MANUSCRIPT

kPa, an unconfined compressive strength of 19.6 kPa, and an internal friction angle of 29.8° were measured, confirming the weak nature of peat and its susceptibility to excessive deformation under load (Çadır et al., 2024; Yalcin et al., 2023).

Combined with its high compressibility, susceptibility to creep, and the uncertain effects of fibrous inclusions, these characteristics make the assessment of foundation stability on peat a challenging task. These unique mechanical properties render peat a notoriously difficult material to work with in construction projects. Consequently, foundation designs typically require higher safety factors or stronger material reduction parameters to account for the unpredictability and complexity of peat's behavior under load (Norazam et al., 2017; Saberian and Rahgozar, 2016; Zwanenburg and Jardine, 2015).

The construction of foundations on soft soils presents significant challenges for designers and contractors. While conventional methods such as soil removal and replacement, piled embankments, and consolidation are commonly used to address these challenges, they are not always feasible due to time constraints, economic limitations, or execution difficulties. As an alternative, advancements in geotechnical engineering have made it possible to improve the bearing capacity of problematic soils on-site using sophisticated machinery and technology. Various techniques are available for enhancing peat and organic soils, including excavation and replacement, preloading, piling, thermal treatment, and chemical stabilization with cement or lime to improve strength and stiffness. Additionally, innovative methods, such as the use of geosynthetics for soil reinforcement, have gained prominence. These include lightweight fill materials and planar reinforcement systems, such as geogrids and geotextiles, which provide efficient and cost-effective solutions for improving soil stability (Akbar et al., 2021; Ghadr and Assadi-Langroudi, 2022; Hosseini et al., 2023; Juneja and Sharma, 2023; Kalyan and Krishna, 2021; Madani et al., 2023; Merse et al., 2023; Shadmand et al., 2018; Shafiee et al., 2024; Talib et al., 2021; Yulianto et al., 2022).

Various types of geosynthetics, including natural fibers, planar geosynthetics, and three-dimensional geocells, are widely employed for soil reinforcement applications (Krishna and Biswas, 2021). Geosynthetics have gained increasing popularity in various geotechnical engineering applications, including ground stabilization beneath fills, pavements, and footings. One of the key applications of these materials is enhancing the bearing capacity and reducing the settlement of foundations. In this regard, numerous studies have explored the effectiveness of geosynthetic reinforcement in improving the performance of footings, investigating the optimal configuration of inclusions to achieve enhanced bearing capacity and settlement behavior. Numerous studies have demonstrated that soil-reinforcement methods are not only cost-effective but also more reliable and efficient compared to traditional ground improvement techniques (Adili et al., 2012; Hejazi et al., 2012; Neto et al., 2013; Tafreshi et al., 2015).

Considerable experimental research has been conducted to investigate the behavior of planar reinforcement in relation to bearing capacity (Abu-Farsakh et al., 2013; Asakereh et al., 2013; El Sawwaf and Nazir, 2012; Fathipour and Payan, 2023; Moghaddas Tafreshi et al., 2011; Prakash K et al., 2023; Useche-Infante et al., 2022). Research has demonstrated that key factors influencing the soil improvement achieved through geosynthetics include the number of reinforcement layers, the spacing between layers, the size of the geosynthetics, and the geometry of the footings (Azzam and Nasr, 2014; El-Sawwaf and Nazir, 2010; Shirazi et al., 2020; Sukmak, 2021; Tafreshi et al., 2015; Yadu and Tripathi, 2013). Numerous studies have investigated the failure modes, settlement

ACCEPTED MANUSCRIPT

behavior, and bearing capacity improvement of geosynthetic-reinforced sand layers placed over soft soils, under both plane strain and axisymmetric conditions, such as strip, circular, and square footings. Extensive research, including laboratory tests and numerical analyses, has been conducted to examine the impact of various factors on the performance of geogrid-supported footings on soft soils (Gedela and Karpurapu, 2021; Roy and Deb, 2017).

To improve soft soils, geotechnical engineers focus on increasing bearing capacity, tensile strength, and overall subsoil performance for more stable and reliable foundations. Over the last three decades, geogrids have been widely utilized to reinforce earth-retaining and earth-supported structures. Their primary functions include reinforcement and separation, enhancing stability, and load distribution (Bhardwaj and Sharma, 2023). The reinforcement of soil using geogrids is a widely adopted technique to enhance shear strength, increase stiffness, and minimize excessive settlements in geotechnical structures, including shallow foundations, retaining walls, and earth slopes. The inclusion of geogrid layers improves the equivalent shear strength of the soil mass, thereby increasing the overall stability of the system. This effect is more significant in weak and soft soils with low strength for construction. Since soil replacement and ground improvement are often costly and time-consuming, reinforcing in-situ soil is a more practical solution. (Yaghoobi et al., 2023).

Among various applications, one effective approach is the incorporation of a geogrid layer between granular fill and soft soil, which has been extensively studied for its impact on shallow foundation performance and bearing capacity. Incorporating a geogrid layer between granular fill and soft soil is an effective technique for improving shallow foundation performance and enhancing ultimate bearing capacity. Extensive experimental, analytical, and numerical studies have explored the response of shallow foundations on geogrid-reinforced sand overlying soft soil (Chenari et al., 2023; Fatehi et al., 2023; Tizpa et al., 2023).

Correctly determining soil behavior is essential to address challenges such as bearing capacity issues, excessive deformation, and settlement problems. While extensive research on soft soil improvement has primarily been conducted in laboratory environments using disturbed soil samples, relying solely on these studies is not always engineeringly feasible (Aminu et al., 2022; Razali et al., 2013; Susanti et al., 2017). The novelty of this paper lies in its use of undisturbed peat samples, ensuring more accurate and relevant results for real-world foundation systems. Unlike previous studies that rely on disturbed peat samples, this research captures the true in-situ properties of peat, offering a more realistic understanding of reinforcement mechanisms and improving the applicability of the findings to actual engineering practices.

Research on undisturbed soil is critical for accurately estimating the behavior of soft soils. Undisturbed block sampling provides reliable data for calculating the settlement and bearing capacity of peat soils. As noted in previous studies, the impact of soil disturbance on soft soils has often been overlooked (Çadır et al., 2024; Kaya and Erol, 2021; Yalcin et al., 2023). Therefore, there is a clear need to investigate the effects of undisturbed peat beds on reinforced sand–soft soil systems. The present study aims to examine the influence of undisturbed soft soil samples on bearing capacity and settlement.

ACCEPTED MANUSCRIPT

This study investigates the potential benefits of using planar reinforcement to enhance the bearing capacity and reduce settlement in square footings placed on undisturbed peat soil. Extensive laboratory tests were conducted using geogrid as planar reinforcement, incorporated within the fill. The bearing capacity analysis considered key parameters of both the sand fill and geosynthetic configurations. To date, few experimental studies have optimized the critical parameters of geogrid reinforcement layers for fills overlying undisturbed peat under isolated footings. The model tests were conducted under optimal conditions to maximize the efficiency of the reinforcing layers. This research aims to address the existing gaps in literature by exploring the effects of geogrid reinforcement on the bearing capacity and settlement behavior of sand beds over peat subgrade, with a particular focus on undisturbed peat samples and their reinforcement with geosynthetics.

A. Framing the Research Problem

The Kayseri Free Zone (KFZ) region, located to the west of Kayseri, Türkiye, is characterized by a significant presence of peat soils. This area is predominantly occupied by industrial buildings, manufacturing facilities, and storage zones, among other infrastructural developments. A review of the structures erected in the region reveals a prevailing preference for shallow isolated footings, primarily driven by the low bearing capacity of the peat soils and the significant settlement observed. This study is principally concerned with examining the potential for soil enhancement in this area through the application of geogrid reinforcement.

This study aims to investigate the bearing capacity and settlement behavior of geogrid-reinforced fills constructed in various configurations, using undisturbed samples of the underlying soft soil layer (UPt) obtained from field sites. UPt samples were collected from designated locations using steel boxes specifically designed by the authors, with dimensions of 750 x 750 x 400 mm. These samples will act as the core material for the laboratory-based construction of sand fills (SP) at two different compaction levels, with relative densities of 45% and 65%. In the testing configuration, geogrid reinforcement is to be incorporated into the SP at varying depth ratios (u/B, h/B), with the length-to-width ratio (L/B) maintained constant. Two distinct geogrid configurations, single-layer reinforcement (N = 1) and double-layer reinforcement (N = 2), are to be systematically evaluated to investigate their impact on the structural integrity and performance of the fill material. The influence of geogrid reinforcement on the bearing capacity and settlement behavior of the SP is set to be assessed using key performance indicators, including the improvement factor and settlement reduction ratio. These parameters are projected to provide critical insights into the effectiveness of geogrid reinforcement in enhancing load-bearing performance and mitigating settlement. To evaluate this, axial and non-eccentric loads will be applied to the peat and fill system, utilizing a highly rigid footing element (20 mm thickness, 80 mm width) to ensure uniform loading conditions.

B. Experimental Investigation

ACCEPTED MANUSCRIPT

B1. Materials used

B1.1 Sand

Conventional laboratory tests were performed to ascertain the physical properties of the soil materials. Prior to testing, measurements were taken for particle gradation, specific gravity, maximum and minimum dry densities, as well as other pertinent physical indices of all soil samples. Laboratory model tests were conducted using clean, dry sand sourced locally from Kayseri, Türkiye. This sand served as the fill material for both unreinforced and reinforced test series. The thickness of the fill layer (H) was adjusted by varying the relative density of the sand layer (D_r) to values of 45% and 65%. The soil utilized in the laboratory tests is classified as medium-sized sand, characterized by rough and angular grains with particle sizes ranging from 0.85 mm to 2.00 mm. In the tests, dry sand with a specific gravity of 2.66 was employed. The maximum and minimum dry unit weights of the sand were determined to be 16.68 kN/m³ and 14.13 kN/m³, respectively. Correspondingly, the maximum and minimum void ratios were found to be 0.847 and 0.566. The sand was maintained in a dry condition, and sieve analysis provided the following grain size parameters: (i) D_{10} = 0.94 mm, (ii) D_{30} = 1.13 mm, (iii) D_{50} = 1.18 mm, (iv) D_{60} = 1.29 mm. The uniformity coefficient (C_u) was calculated to be 1.37, and the coefficient of curvature (C_c) was found to be 1.05. Here, D_{10}, D_{30}, and D_{60} represent the particle sizes below which 10%, 30%, and 60% of the mass, respectively, falls. Upon calculation, the C_u was calculated to be 1.37 ($C_u < 6$), and the C_c was measured at 1.05, falling within the range of 1 to 3. These coefficients confirm that the dry sand is classified as poorly graded. Shear strength parameters were assessed using a standard direct shear box (100×100×25 mm) for dry sand samples. A series of direct shear tests were performed on the fill material at relative densities of 45% and 65%. The internal friction angles obtained from the direct shear tests (ϕ_{ds}), specifically 34.3° and 36.1°, were subsequently converted into triaxial test values using the equation provided below (Eq. 1). The computed triaxial friction angles (ϕ_{tr}) were then defined as 34.2° and 35.4°, respectively (Lade and Lee, 1976).

$$\phi_{tr} = \left(\phi_{ps} + 17°\right)/1.5 \quad (1)$$

Table 1 presents the physical properties of the sand, indicating that the relatively uniform soil used in this paper can be classified as poorly graded sand (SP) according to the Unified Soil Classification System.

(Table 1 here)

B1.2 Peat

Undisturbed peat samples were collected from the KFZ, which spans approximately 7 million square meters within the boundaries of Kayseri Province, Turkey. Fig.1 illustrates the combination of silty clay and topsoil found at the surface, with depths ranging

ACCEPTED MANUSCRIPT

between 0.30 and 0.50 meters. Beneath this layer, peat deposits extend to a depth of around 8 meters, with clay bands present near the surface, ranging in thickness from 0.05 to 0.20 meters. The uppermost portion of the peat deposit, extending from the surface to about 1.90 meters, consists of sedges, plant roots, coarse fibers, and some silty clayey material. Further down, the peat becomes finer and more amorphous in nature. At greater depths, beneath the peat deposits, layers of silty sand and low-plasticity clay are encountered, offering additional geological insight into the site's stratigraphy.

(Fig. 1 here)

A test pit (TP-1) was excavated to obtain both disturbed and undisturbed peat samples for further analysis. Index tests were carried out on the undisturbed samples to determine key soil properties. Laboratory testing was conducted to assess the physical and mechanical properties of the peat and its components. These tests included determining parameters such as moisture content, grain size distribution, organic content, and shear strength, which are essential for understanding the material's behavior and its suitability for engineering purposes. Table 2 presents a summary of the test outcomes, including the methods employed, the parameters measured, and the corresponding values for disturbed and undisturbed samples.

(Table 2 here)

B1.2.1 Technique in peat soil sampling

Undisturbed soil samples were collected from depths ranging between 1.80 m and 2.80 m below the ground surface. Thirty test boxes were used for on-site sampling, and these were driven into the soil with the assistance of a backhoe-loading machine. During the sampling process, two distinct soil layers were identified, with a measured elevation difference of 0.80 m. The first layer was subjected to the burial process, with the lower portions of the test boxes placed in contact with its surface. The figure presented below (Fig. 2) depicts the excavation procedure to the designated depth from the surface, followed by the installation of the test box into the peat soil.

(Fig. 2 here)

ACCEPTED MANUSCRIPT

The test boxes were custom-designed by the authors. These boxes were constructed from 10-mm thick steel and consisted of three components: the main body, the top cover, and the lower sled. Several design enhancements were incorporated to minimize soil disturbance during sample collection. The top cover was reinforced to prevent deformation during insertion, as force was applied to push the box into the soil. Air holes were incorporated into the top cover to allow the release of trapped air during the uniaxial downward push, facilitating the easy entry of peat soil into the main body of the box. Additionally, the lower part of the test box was beveled at a 30° angle to promote easier penetration into the soil, reducing disturbance and ensuring a "knife effect" for smoother insertion. All connections between the top cover and lower sled, including screws and sliding elements, were carefully inspected to prevent any potential discontinuities. To prevent contamination or loss of material, the test boxes were securely wrapped in stretch plastic film and labeled appropriately. They were then promptly transported to the laboratory for further analysis.

The design of the test boxes was specifically developed to extract peat samples with minimal disturbance to the surrounding soil. To minimize soil disturbance, careful handling was ensured throughout the procedure. First, the topsoil was cleared, and gradual excavation was carried out to a depth of 0.80 m above the groundwater level. In the following stage, the bottom sled of each test box was removed, and the boxes were placed on the peat at horizontal intervals of 1.00 m. In the third phase, the boxes were pushed into the soil, allowing the peat to enter the boxes. Finally, the bottom sled was replaced, and the test boxes were carefully extracted, wrapped in nylon covers, and transported to the laboratory with utmost care to preserve the integrity of the samples.

B1.2.2 Soil disturbance assessment

Several methods for assessing sample quality have been proposed by researchers, with studies indicating that mechanical disturbance is much greater in tube samples than in block samples (Amundsen et al., 2016; Andresen and Kolstad, 1979; Hajj, 1990; Karlsrud and Hernandez-Martinez, 2013; Nagaraj et al., 1990; Terzaghi et al., 1996). This study employs three distinct methods for assessing sample disturbance, as outlined by Andresen and Kolstad, Lunne et al. and, Karlsrud and Hernandez-Martinez to evaluate sample disturbance.

Sample quality is often assessed using volumetric strain (ε_v), which measures the relative volume reduction during consolidation (Andresen and Kolstad, 1979). Lunne et al. proposed an alternative method based on changes in the void ratio ($\Delta e/e_0$) relative to the initial void ratio (e_0) and the over-consolidation ratio (OCR). In this method, Δe represents the change in void ratio due to the in-situ effective stress (σ'_{v0}). This approach is widely recommended by the Norwegian Geotechnical Society (NGF, 2012). Karlsrud and Hernandez-Martinez introduced a further criterion, the oedometer stiffness ratio (M_0/M_L), calculated from consolidation tests, where M_0 is the maximum constrained modulus within the over-consolidated stress range, and M_L is the minimum modulus after pre-consolidation. The degree of sample disturbance is evaluated using these three methods, each employing specific parameters and criteria, as shown in Table 3.

ACCEPTED MANUSCRIPT

(Table 3 here)

According to Lunne et al., the assessment of sample disturbance quality is based on the parameters $\Delta e/e_0$ and OCR. In this study, consolidation tests were conducted by ASTM D2435 standards (ASTM, 2020). The ε_v ranged from 0.03 to 0.71, while $\Delta e/e_0$ and OCR values ranged from 0.008 to 0.023 and 1.61 to 1.90 (OCR=1-2), respectively. The M_0/M_L ratio ranged from 1.95 to 2.87, a range that aligns with the classification scheme established by Karlsrud and Hernandez-Martinez. Based on these results, the peat sample, extracted as a block from the study site, was classified as having a 'very good to excellent' quality, as per the criteria in Table 3.

The design and construction of the sample boxes were carefully optimized to minimize disturbance during the extraction process. The boxes were engineered for structural rigidity to withstand the forces applied during insertion, while their sharp edges facilitated smooth penetration into the soil, thereby ensuring the preservation of sample integrity throughout the collection procedure.

The degree of disturbance in block sampling of soft soils is a paramount consideration. In the present investigation, the test boxes were constructed with a thickness of 10 mm to provide adequate rigidity against bending moments during the insertion and extraction of roughly 300 kg of peat soil. The specified thickness was determined through computer-aided solid modeling analysis to ensure optimal performance. Furthermore, the cutting edges of the sample boxes were precisely sharpened, similar to those of thin-walled tubes, to facilitate smooth penetration into the soil, thereby ensuring undisturbed sampling. The degree of disturbance in the samples, obtained through various sampling methods, can be quantified using the area ratio (A_r), a parameter frequently employed in thin-walled tube sampling techniques (ASTM, 2000), as presented below:

$$A_r = \frac{D_o^{\,2} - D_i^{\,2}}{D_i^{\,2}} \tag{2}$$

where D_i is the inner diameter of the cutting edge, D_o is the outer diameter of the cutting edge. The integrity of a soil sample is typically considered undisturbed when the area ratio (A_r) is below 10%. Based on Eq. 2, the calculated A_r value for the peat samples in this paper is 2.7%, indicating that the peat samples can be classified as undisturbed.

B1.3 Footing

A square rigid steel plate with a thickness of 20 mm and side lengths of 80 mm was chosen as the footing for the reduced-scale model. This selection was based on the consideration that the vertical stresses generated beneath the footing diminish at a distance of 3.5B from the base, and do not overlap with the base of the test box, while the horizontal stresses decay at a distance of 1.5B, ensuring no overlap with the walls of the test box, as described by Boussinesq's approach (Bowles, 1997). Jong-Seok conducted laboratory model tests to evaluate Boussinesq's theory on vertical stress increments due to surface loading. The results showed that

ACCEPTED MANUSCRIPT

theoretical stress values were consistently lower than measured values beneath the footing, regardless of depth. This highlights the limitations of theoretical models in capturing granular soil behavior, justifying the adoption of a slightly greater fill depth to account for deviations from theoretical predictions (Jong-Seok, 2004).

To ensure that the rupture zone remains entirely within the test box, the plan dimensions of the box should be at least five times the length of the footing (Akhil et al., 2022). However, the steep stress gradients beyond the rupture planes suggest that the stresses will change negligibly once the test box boundary is reached. Although the pressure distribution due to the footing is expected to extend somewhat beyond 25% of the box depth and 40–50% of the box width, as indicated by Panagiotidou et al., the boundary effects are minimized by maintaining the footing width at less than 1/5 of the test box width in the physical model (Li-Hua et al., 2022; Panagiotidou, 2010).

The footing's 20 mm thickness ensures that it functions as a rigid, solid plate, unaffected by bending deformations. A thin layer of sand was applied to the base of the footing using epoxy adhesive to enhance the roughness of the footing surface. The sides of the steel footing were kept smooth to minimize additional skin friction resistance. The rigid footing was utilized to transfer vertical loads, as depicted in Fig. 3.

(Fig. 3 here)

The footing load was measured using a pre-calibrated load cell, which was mounted on a hydraulically operated jack and supported by a rigid reaction frame. The load was applied vertically through a shaft positioned in a groove on the upper surface of the footing. To ensure the load remained vertical during application and to monitor any potential tilting or rocking of the footing, a lubricated loading shaft was employed. This shaft was shaped as a half-sphere and seated at the center of the footing. It was critical to ensure proper alignment between the center of the footing and the loading shaft during the connection process. The gap between the groove and the vertical cylindrical shaft was minimal, and the experimental setup was designed to prevent any tilting of the footing during loading. Additionally, prior to initiating the axial loading, the alignment between the center of the footing and the center of the test box was carefully confirmed. Throughout the tests, the axial load was applied while ensuring the verticality of the footing to prevent any eccentricity in the applied load (Kumar and Khatri, 2008). The surface of the sand bed was precisely leveled, and the square footing was placed at the center of the leveled surface. The particle size of the sand relative to the footing width, often referred to as the "particle size effect", can influence the bearing capacity (Ovesen, 1979; Tatsuoka et al., 1991). The ratio of the particle size to the footing width, D_{50}/B, which decreases as the footing width increases, may affect the bearing capacity. Kusakabe summarized test data from the literature and indicated that the particle size effect on bearing capacity becomes less pronounced for the D_{50}/B ratio between 1/50 and 1/100 (Kusakabe, 1995). This suggests that the particle size effect in the present study is likely to be minimal.

ACCEPTED MANUSCRIPT

For the value of D_{50}=1.18 mm in this work, the D_{50}/B ratio was approximately 1/67.8 for a footing width of 80 mm, indicating that the effect of grain size did not significantly influence the results (Okamura et al., 2002).

B1.4 Geogrids

The geogrid used in this study is composed of alkali-resistant glass fibers, selected for their enhanced durability and resistance to degradation in alkaline environments, such as high-pH soils or concrete subgrades. These fibers are particularly advantageous for reinforcement applications where conventional fibers may deteriorate due to chemical interactions with the surrounding materials, ensuring long-term structural stability and performance (Sharo et al., 2022).

Within the framework of this inquiry, a geogrid designated as FT160, made from polymer E-glass (alkali-resistant glass fibers), was utilized. Manufactured by İstanbul Teknik Geoteknik (Türkiye), the geogrid has a unit weight of 160 g/m² and a square-shaped aperture with a mesh size of 4.0 × 4.0 mm. The tensile force measured at 2% axial strain was approximately 29.1 kN/m, while the ultimate tensile strength was determined to be 38.6 kN/m.

To evaluate the suitability of the selected geogrid for 1g model testing, its tensile strength was compared with representative values reported in the literature. Demir et al. reported an ultimate tensile strength of 60.0 kN/m (Demir et al., 2013), Mehrjardi and Khazaei documented a range of 30.0–83.6 kN/m (Mehrjardi and Khazaei, 2017), and Bathurst and Naftchali compiled values ranging from 38.0 to 177.0 kN/m (Bathurst and Naftchali, 2021). These comparisons suggest that the geogrid employed in this study falls within an empirically supported range for physical modeling, thereby reinforcing its validity as a model reinforcement material.

This particular type of geogrid exhibits uniform tensile strength across all directions. The material properties of the reinforcement are also outlined in Table 4, as provided by the manufacturers. Table 4 summarizes the essential properties of the geogrid, which were determined using a universal testing machine. A specimen of the geogrid was subjected to a wide-with tensile test, as per the specifications outlined in EN ISO 10319 standard (ISO, 2024).

(Table 4 here)

Geogrid tensile strength plays a critical role in soil reinforcement applications, as it affects load distribution, soil confinement, and overall stability. However, studies indicate that beyond a certain threshold, increasing tensile strength does not proportionally enhance the improvement factor in terms of bearing capacity and settlement reduction (Al-Barqawi et al., 2021; Derksen et al., 2022; Krishna and Biswas, 2021). This is attributed to the fact that once a geogrid has reached strain compatibility with the surrounding soil, further increases in tensile strength do not lead to a significant mobilization of additional tensile forces (Liu et al., 2014). Determining the optimal tensile strength for geogrid selection requires balancing reinforcement effectiveness with economic

ACCEPTED MANUSCRIPT

feasibility. While higher tensile strengths can improve stiffness, they do not necessarily enhance performance beyond a certain point and may lead to unnecessary costs. Conversely, insufficient tensile strength may result in premature failure or inadequate reinforcement mobilization (Wulandari and Tjandra, 2006). In our study, the selected geogrid tensile strength was chosen based on the required strain compatibility for the test conditions, ensuring adequate reinforcement mobilization without excessive stiffness.

In this research, the ultimate tensile strength of the geogrid is relatively low because the laboratory tests have been conducted by using small-scale physical modeling. When a small footing width is used, it is suitable to utilize geogrid reinforcement with a low tensile strength and small aperture sizes to allow the interaction between the soil and geogrid used to achieve good performance (Ahmad, 2022). The use of FT160 is intended to reduce the tensile strength of the reinforcing layer for model tests, as weaker geogrids are not available for fabrication. A weaker biaxial geogrid exhibits a secant modulus approximately one-third that of a stronger biaxial geogrid, indicating significantly lower stiffness. (Latha et al., 2013). Fig. 4 presents the geogrid (FT160) employed in the experimental testing process.

(Fig. 4 here)

Another critical selection criterion was aperture size, which governs soil-geogrid interlocking and load transfer efficiency, particularly in small-scale model tests (Özer, 2021). To optimize reinforcement performance, the nominal aperture size is typically recommended to be four times the median grain size (D_{50}) of the fill material. Given that the D_{50} in this study is 1.18 mm, the ideal aperture size is estimated to be 4.72 mm. The selected geogrid, with a 4.0 mm aperture, closely aligns with this recommendation, ensuring effective soil confinement and stress distribution while maintaining realistic reinforcement behavior in granular fill (Mehrjardi and Khazaei, 2017).

The material composition of the geogrid was chosen for its durability and compatibility with the test conditions, particularly for reinforcing granular fill over soft soil. Its resistance to degradation and ability to withstand high tensile stresses ensure reliable performance in geotechnical applications, including shallow foundation reinforcement on soft soils (Mittal and Shukla, 2018). These properties validate the experimental setup and enhance the geogrid's effectiveness in improving bearing capacity and settlement reduction under sustained loading.

All model tests involving reinforcement were carefully placed at the designated depth, specifically at 0.2B and 0.3B (for the first reinforcement layer) below the base of the footing, as per the test parameters.

B2. Test apparatus and instrumentation

ACCEPTED MANUSCRIPT

The effect of geogrids on the bearing capacity of sand over undisturbed peat soil (UPt) was investigated using a test box (TB2) with internal dimensions of 750 mm in length, 750 mm in width, and 400 mm in depth. The dimensions were selected based on a review of relevant literature and the results of finite element (FE) analysis to ensure their suitability for the model tests. The inner walls and edges of the TB2 box were coated with lubricated oil to minimize friction as much as possible.

The axial load applied to the footing was precisely measured using a pre-calibrated load cell positioned between the footing and the hydraulic jack. A computer-controlled hydraulic jack was employed to regulate the loading process, ensuring precise control over the applied load. This hydraulic jack was connected to both the loading frame and the physical model tank via screws, facilitating uniform load application to the footing. A 50 kN capacity load cell, with an accuracy of ± 0.02%, was placed between the reaction frame and loading rod to continuously record the vertical pressure applied to the loading steel plate. For settlement measurements, a Linear Variable Differential Transformer (LVDT) with a maximum travel of 300 mm and an accuracy of 0.01 mm was utilized. The LVDT (LVDT0) recorded the settlement of the loading plate throughout the test. The loading rod is mounted onto the hydraulic jack via a universal shaft, ensuring efficient load transmission during the test. The universal shaft is coated with lubricating oil to minimize friction between the shaft and its surface, thereby facilitating smoother operation during the loading process. During the loading process, the loading rod was maintained in a vertical orientation to prevent tilting of the footing. A ball-bearing arrangement was employed to ensure uniform load transfer and eliminate any eccentricity in the applied load. The footing was precisely aligned at a predetermined position atop the sand bed. Four LVDTs (LVDT1, LVDT2, LVDT3, and LVDT4) were strategically positioned at distances of 1.5 and 2.5 times the footing width from its centerline, on either side, to monitor surface heave during the test as outlined (Latha and Somwanshi, 2009). The figure below (Fig. 5) illustrates the accurate positioning of LVDTs for monitoring surface heave at defined distances from the footing centerline.

(Fig. 5 here)

The schematic in the following figure (Fig. 6) illustrates the testing setup, emphasizing the configuration of key instrumentation used to measure load and displacement during the testing process.

(Fig. 6 here)

The load cell and LVDTs were calibrated and operated in the laboratory to ensure the reliability and accuracy of the recorded measurements. All output data from the instrumentation were continuously recorded and collected using a twelve-channel digital data logger. Prior to each test, all measurement devices were carefully calibrated to ensure accurate and reliable readings. Load and

ACCEPTED MANUSCRIPT

displacement measurements were digitally recorded and transmitted to a computer via the data logger for further analysis. After the completion of the first model test, all soil samples and testing equipment were removed from the test boxes. The properties of the soft subgrade soil and fill were maintained unchanged for the second model test to facilitate a direct comparison between the two configurations.

B3. Soil preparation

A soil sample was prepared for a two-layered system, where a sand fill was placed over a soft underlying layer (UPt). Details regarding the sampling of the underlying UPt are briefly discussed in the 'Peat' section. Following the peat soil sampling, the thickness of the top layer (TB1) was fixed at 450 mm. The depth of the SP (in TB2) was varied at two different values: 160 mm (denoted as H=2.0B) and 320 mm (denoted as H=4.0B). Experimental tests were conducted on the SP at relative densities (D_r) of 45% and 65%, yielding corresponding unit weights of 15.16 kN/m³ and 15.68 kN/m³, respectively.

The selected relative densities were determined based on geotechnical literature and experimental feasibility to optimize bearing capacity while ensuring practical constructability (Das, 2013; Holtz et al., 2011). Densities below 30% result in excessive settlement, whereas densities above 70% are constrained by compaction limitations and an increased risk of particle breakage (Tatsuoka et al., 1991; Yetimoglu et al., 1994). The chosen values strike a balance between field applicability and experimental consistency, ensuring reliable reinforcement performance.

The SP was placed within the TB2 at 45% and 65% relative densities, with specific methodologies applied to ensure uniformity and accuracy. For D_r = 45%, the sand raining method was solely employed, following Srinivasan and Ghosh, to achieve homogeneous deposition without additional compaction (Srinivasan and Ghosh, 2012). To maintain uniformity in the sand fill, the surface of the sand was leveled using a steel ruler before placing reinforcements at their predetermined positions. The sand deposition process continued using the sand raining technique until the footing level was reached, ensuring that the fill density remained consistent throughout the layering process. For D_r = 65%, preliminary trials demonstrated that sand raining method was insufficient to reach the target density. Therefore, a weight–volume method was adopted, where sand was placed in layers and compacted using a predefined number of blows. To further refine the process, an electrically operated vibration-based compaction method, as outlined by Keskin et al., was employed. This technique ensured uniform densification while minimizing particle crushing, with a steel plate distributing force evenly. The placement height was meticulously controlled using scaled markings on the test box, and post-compaction leveling was performed to establish uniform load distribution beneath the model footing. Control tests confirmed that density variations remained below 1%, validating the consistency and reliability of the prepared sand bed (Keskin et al., 2023).

Achieving 65% relative density in field applications is challenging due to equipment constraints and potential subgrade disturbance (Holtz et al., 2011; Indraratna et al., 2012). A 50%–60% density range is more practical, as excessive compaction can cause pore

ACCEPTED MANUSCRIPT

pressure buildup, strength loss, and differential settlement (Mayne et al., 2002; Terzaghi et al., 1996). High-energy compaction may also induce vibrations, destabilizing adjacent structures (Tatsuoka et al., 1991).

The weight of each sand layer was precisely calculated to achieve the desired compaction, with 34.9 kg for D_r = 45% and 36.0 kg for D_r = 65%, based on the dry density of the SP material. The degree of compaction was a critical quality control parameter in this testing program, directly influencing the reliability of the results. To ensure consistency in compaction across layers, the dry density of the SP fill was regularly calculated and monitored. For each layer, which was uniformly 40 mm thick, the required mass of sand was precisely determined based on the maximum dry density of the material, ensuring that the desired compaction level was achieved for every layer. The reinforcing materials and LVDTs were placed at predetermined depths, as previously described. After each test, the TB2 was evacuated and refilled to maintain consistency between experimental runs.

B4. Test Procedures

B4.1 Test variables

Due to their cost-effectiveness and efficiency in terms of time, laboratory-reduced model tests have become a predominant method for investigating geosynthetic-reinforced soil foundations. The equipment typically used for conducting plate load tests includes a test box, loading apparatus, rigid footing, and LVDTs. Based on these small-scale model tests, the impact of various factors on the bearing capacity and settlement behavior of reinforced foundations has been extensively analyzed. Key factors influencing these parameters include layout configurations, footing size, and the characteristics of the foundation soil. At present, researchers primarily assess the effect of these factors on the footing's bearing performance by comparing the load-settlement curves of unreinforced and reinforced foundations.

As part of the reinforcement studies, all the variables to be tested were initially determined using finite element analysis (FEA) methods. The challenges associated with obtaining large undisturbed samples, along with the necessity of employing separate test boxes within the UPt for each loading test, constrained the number of laboratory-scale experiments that could be conducted. In light of these constraints, parameters such as N, H, u, and h were first selected over a broad range, and subsequent finite element analyses were employed to narrow down the value ranges, ultimately leading to the determination of the final parameters.

The layout parameters of the reinforcement materials (e.g., geogrid) in reinforced footings include the depth of the fill layer (H), the distance between the top reinforcement layer and the base of the footing (u), the spacing between reinforcement layers (h), the length of reinforcement (L), the number of reinforcement layers (N), and the depth of the reinforced zone (d_r). To facilitate the comparison

ACCEPTED MANUSCRIPT

of various influencing factors, all parameters, except for N, are expressed in dimensionless form by normalizing them with respect to the footing width (B), i.e., u/B, h/B, L/B, and d/B (Guo et al., 2020). Table 5 outlines key reduced-scale model tests conducted on geosynthetic-reinforced foundations, along with their corresponding optimal layout parameters.

(Table 5 here)

According to the published literature and results from Table 5, the optimum layout parameters for the reinforced foundation can be summarized as follows:

(1) For the top reinforcement layer, the optimal embedment depth (u/B) typically ranges from 0.3 to 0.4. If u/B is too small, the reinforcement may not be adequately anchored by the overlying soil. On the other hand, an excessively large u/B may lead to shallow shear failure above the top reinforcement layer, compromising the enhancement of bearing capacity (Ghosh et al., 2005). To evaluate the optimal depth for maximum strength enhancement, the embedment depth of the single-layer geogrid was chosen as 0.2 and 0.3 times the footing width. This embedment depth (u) was also expressed as a ratio of the footing width (Apurva et al., 2022). For the purposes of this study, u/B values of 0.20 and 0.30 were adopted.

(2) An optimal vertical spacing for the reinforcement, denoted as h/B, exists within the effective reinforced depth. The bearing capacity improves as h/B decreases but begins to decline when h/B falls below a critical threshold (Yetimoglu et al., 1994). The recommended range for h/B is approximately 0.2 to 0.4. For this paper, the value of h/B was selected as 0.20 and 0.30.

(3) The bearing capacity of a soil foundation increases with the reinforcement length (L/B). However, once L/B exceeds a critical value, further increases in reinforcement length have a minimal impact on performance. This is because, beyond the effective anchorage zone, the frictional resistance and passive forces provided by the reinforcement have a limited effect on enhancing bearing capacity (Das and Omar, 1994; Shin et al., 1993). The optimal L/B is typically recommended to range from 4 to 5. To provide clarity, L/B is maintained constant at 5 in the current work.

(4) The bearing capacity of the footing increases with reinforced depth (d_r). However, beyond a certain depth, further increases in 'd_r' do not significantly enhance bearing capacity (Latha and Somwanshi, 2009). Based on these insights, the d_r value was selected between 0.2B and 0.6B for the present study.

The test results of bearing pressure (q) against normalized footing settlement (s/B), nondimensional surface deformation (d/B) against normalized distance from the base center (l/B) are presented and analyzed. 's' is the footing settlement, 'd' represents the

ACCEPTED MANUSCRIPT

fill surface deformation and 'l' is the horizontal distance from the footing center. All parameters are expressed by dimensionless parameters to minimize the scale effects such as s/B and d/B (Mittal and Gill, 2020).

To compare the results, a new variable has been defined which gives the stress ratio of the stresses which must be applied to the foundation to create the same amount of settlement in the reinforced and unreinforced soil. This variable is called the improvement factor (IF). In general, IF and the percentage reduction in settlement ratio (PRS) were used as dimensionless parameters to evaluate the reinforcement effectiveness of the geogrid. The IF is defined as follows (Eq. 3):

$$IF = \frac{q_r}{q_u} \tag{3}$$

where q_r, is the bearing capacity of reinforced foundation as the footing reaches a certain settlement, q_u is the bearing capacity of unreinforced footing when the footing reaches the same settlement. PRS is defined as follows (Eq. 4):

$$PRS = \frac{(s_u - s_r)}{s_u} \times 100 \tag{4}$$

where s_r is the footing settlement in reinforced footing under a certain load, and s_u is the footing settlement in unreinforced footing under the same load.

B4.2 Testing strategy

A total of 29 tests (excluding repetitions) were conducted as part of the complete experimental program, which included four different test series: one uniform configuration (T0 test) and three-layered configurations (T1, T2, and T3). The experimental program initially focused on footings resting on unreinforced sand beds overlying UPt, after which the effect of reinforcement on the sand beds was subsequently investigated. In these tests, the H/B ratio was maintained at 2.0 and 4.0. Harikumar et al. examined geosynthetic-reinforced foundations and concluded that the reinforcement width did not significantly affect the bearing capacity when it exceeded 4B (Harikumar et al., 2016). The study involved a series of plate load tests conducted on square footings placed on geogrid-reinforced sand beds with relative densities of 45% and 65%. Model tests were performed using square footings with a width (B) of 80 mm, placed on the geogrid-reinforced sand bed. The primary parameters investigated included bearing capacity for each test and the footing settlement (s), which was normalized to the footing width (B). As mentioned in the previous section, the appropriate values for the variables in the test programs were determined through preliminary analyses conducted using FEA.

The test results indicated that bearing pressure increased nonlinearly with footing settlements, continuing until the tests were completed (s/B ≈ 30%). To ensure the reliability and reproducibility of the results, several replicate installations were carried out, verifying the consistency of loading performance, instrumentation, and applied loading control.

ACCEPTED MANUSCRIPT

The response of the model footing on unreinforced UPt was investigated in the T0 test. Tests on reinforced sand beds overlying UPt were categorized into three distinct series. In the T1 series, the bearing capacity of the fill, constructed at different densities, was evaluated and compared to the uniform UPt soil. No reinforcement elements were employed in either the T0 or T1 tests. The T2 series focused on determining the bearing capacity of the first layer of reinforcement (N=1). These tests were performed using a single layer of reinforcement, with varying u/B values of 0.2 and 0.3. In the T3 series, for N = 2, different configurations were tested with u/B values of 0.2 and 0.3, and h/B values of 0.2 and 0.3, to investigate their effects on bearing capacity. Table 6 depicts the details of the parameters considered in the experimental program. The results and detailed observations for each test series (T0–T3) are discussed in the Results section.

(Table 6 here)

Table 6 presents the reinforcement conditions tested in this study, designed to evaluate the effects of reinforcement placement, relative density, and geogrid layering on load-bearing capacity and settlement behavior. The T0 series served as a baseline, representing unreinforced soil conditions. The T1 series, without geogrid reinforcement, assessed the influence of sand fill thickness and relative density on soil behavior. The T2 series examined the effect of a single geogrid layer at different depths on load distribution and soil confinement. The T3 series evaluated double-layer reinforcement with varying vertical spacing to identify optimal stabilization strategies.

The experimental setup for the tests is described as follows. The test box was positioned beneath a loading frame, and after leveling the UPt bed, sand was used to construct fills of 160 mm and 320 mm in height (H = 2B and H = 4B, respectively). Fig. 7 presents the configurations of the boxes subjected to axial loading schematically.

(Fig. 7 here)

All tests were conducted in a strain-controlled manner with a constant displacement rate of 1 mm/min, ensuring compliance with ASTM D1196M (ASTM, 2012).

B4.3 Scaling effects in physical modeling

Physical modeling is a widely utilized technique for investigating specific aspects of prototype behavior. While full-scale testing can be viewed as a form of physical modeling, where the prototype is reproduced in its entirety, most physical models are constructed at reduced scales. This reduction in scale offers the advantage of faster data acquisition and greater control over model details, which

ACCEPTED MANUSCRIPT

would be difficult to achieve with full-scale experiments. This is especially true in the context of 1-g model tests, which are commonly used to study large deformation problems, where scaling plays a crucial role (Wood, 2004).

Through the variation of key parameters in scaled models, researchers can gain a deeper understanding of their effects and explore expected response patterns. This approach often requires conducting numerous model tests and, in many cases, repeating individual tests to ensure the reliability of the results. The ability to perform parametric studies and adjust model parameters provides insights that contribute to more efficient experimental processes when compared to full-scale testing. As noted by Wood (2004), one of the primary advantages of using scaled physical models is the ability to obtain reliable data more rapidly, while maintaining close control over experimental details—a feat that would be far more challenging in full-scale testing (Salamatpoor et al., 2018).

Despite the widespread application of physical models to simulate prototype behavior, it is well-known that most laboratory tests involve small-scale footings (Ghosh et al., 2005; Guido et al., 1986; Sitharam and Sireesh, 2004; Yetimoglu et al., 1994). In contrast, footings in field conditions are significantly larger. As a result, model tests conducted under normal gravity (1-g) do not fully replicate the real behavior of the soil, due to the dominant influence of the self-weight forces of the soil (Mehrjardi and Khazaei, 2017; Useche-Infante et al., 2023; Viswanadham and König, 2004). Therefore, it is essential that laboratory test results can predict the actual behavior of full-scale prototypes. According to Wood (2004), successfully replicating the behavior of prototype footings in model tests requires more than just maintaining geometrical similarity; it is also crucial to ensure that stress and settlement conditions are consistent between the model and prototype (Buragadda and Thyagaraj, 2019). Langhaar's scaling law defines how material stiffness and other parameters must be adjusted in scaled models. Reinforcement stiffness should increase by λ^2, where λ is the scaling factor between the model and the full-scale footing width. Similarly, geometric parameters, including soil shear modulus, scale by λ to preserve stress similarity (Langhaar, 1951).

In alignment with the scaling laws proposed by Wood [36], the model footings, consisting of rigid steel plates with dimensions of 80 mm in length and width, are scaled by a factor of 40 to represent the concrete prototype footings, which measure 3200 mm in both length and width. In the context of this paper, scaling factors for the geogrid were applied to minimize the risk of overestimating the reinforcement effect in the interpretation of the test results. The relationship between the model and the prototype is governed by the scaling laws, as detailed in Table 7. These laws provide a structured approach for extrapolating the results of the model to the prototype, ensuring that the findings are both relevant and applicable to practical applications.

(Table 7 here)

Achieving perfect mechanical similitude in scaled geotechnical model tests is inherently limited by material availability and testing constraints. For instance, scaling from an 80 mm model footing to a 3200 mm full-scale prototype would theoretically require a

ACCEPTED MANUSCRIPT

1600-fold increase in reinforcement stiffness, which is beyond the capabilities of commercially available geosynthetics. Instead of strict stiffness scaling, physical modeling often emphasizes behavioral similarity under equivalent boundary conditions and relative stiffness ratios. As noted by Viswanadham and König, perfect scaling is rarely feasible, and small-scale models typically prioritize realistic mobilization and interaction trends over exact mechanical equivalence (Viswanadham and König, 2004).

C. Results

This section provides a comprehensive analysis of the influence of various parameters on the bearing capacity of footings, supported by experimental data. A detailed comparison of the pressure-settlement response for both reinforced and unreinforced conditions is presented, with an emphasis on quantifying the improvement in bearing capacity due to geogrid reinforcement. Table 8 below summarizes the details and parameters for all the loading tests conducted in this paper.

(Table 8 here)

When a loading test is conducted for soft soils, local shear failure occurs in general. However, if geogrids and a sand layer are laid at the upper part of the soft soil, the form of failure becomes significantly different, which illustrates the trend of continuous increase in applied pressure (q) vs. footing settlement (s). In this scenario, researchers are unable to obtain ultimate bearing capacity, as they cannot point to the peak value (q_{peak}). When q_{peak} is not clearly observed, it is important to note here that the ultimate bearing capacity is determined from the q-s plots by employing the various procedures suggested by researchers (Akbar et al., 2021; Cerato and Lutenegger, 2007; Park et al., 2013). In these approaches, q_u is considered as the point on the q–s curve at the time when the width of the footing settled by 5%, 10%, and 30%. For consistency, the ultimate bearing capacity is defined as the stress corresponding to a footing displacement of 10% of the footing width.

The load-displacement curves in the current study exhibited characteristics of local or punching-type failures, rather than general shear failure. Local shear failure occurs in footings placed on the sand with medium density ($36\% < D_r < 70\%$) while punching shear failure is observed in unreinforced UPt. These observed failure modes are compared with the classical model for general shear failure proposed by Terzaghi. Terzaghi also suggested adjusting the friction angle, ϕ, to $2/3\phi$ when local shear failure occurs. However, he did not address punching shear failure in his original work (Cerato and Lutenegger, 2007). A testing program was developed to investigate the effects of random variables on isolated square footings under axial loads. The results revealed that load-displacement behavior was independent of relative sand density, exhibiting an initial elastic response, followed by a confined plastic phase, and culminating in impending plastic deformation at failure (El Wakil, 2010).

ACCEPTED MANUSCRIPT

To assess the performance of isolated footings on unreinforced and geogrid-reinforced fill, improvements in bearing capacity and settlement are quantified using non-dimensional improvement factors relative to the ultimate bearing capacity and different levels of footing settlement. As the applied load increased, the settlement reached 30% of the footing width. The improvement in bearing capacity was assessed using non-dimensional factors, including IF and PRS, as defined in the previous sections. These factors quantify the increase in bearing capacity and are consistent with methodologies from prior research (Al-Haddad et al., 2022; Apurva et al., 2022; Harikumar et al., 2020; Kargar and Hosseini, 2017). The behavior of footings on layered soil strata, in comparison to homogeneous strata, as well as the performance of reinforced layered strata versus unreinforced layered soil, is quantified by analyzing the pressure-settlement responses through improvement factors such as IF_0, IF_1, IF_2, IF_3, and IF_4. A comprehensive summary of all data related to these improvement factors is presented in Table 9.

(Table 9 here)

The results indicated that as load-bearing pressure increased, settlement also increased across all embedment depths and relative densities. However, bearing capacity improved with increased embedment depth for all relative densities, and relative density increases (from 45% to 65%) further enhanced bearing capacity. This can be attributed to the greater strength of the fill under higher embedment depth and density, which enables the soil to withstand higher loads (Kuranchie et al., 2016). The experimental results demonstrated a substantial reduction in settlement for the geogrid-reinforced soil bed when compared to the unreinforced soil bed. These results are consistent with previous studies, which have similarly shown that geogrid reinforcement significantly improves the performance of soil under load. These findings underscore the effectiveness of geogrid reinforcement in enhancing the load-bearing capacity and reducing settlement in geotechnical applications, further validating the use of geogrids in improving soil performance under axial loading conditions.

C1. Homogenous subgrade

Various methods have been proposed for calculating bearing capacity, including the 0.1B, log-log method (LLM), tangent-intersect method (TIM), and the hyperbolic method (HM). Among these approaches, the 0.1B method is considered particularly reliable, especially when analyzing failure curves resulting from load-induced failure (Kaya and Erol, 2021; Yalcin et al., 2023). Therefore, in this study, the 0.1B method was adopted to determine the ultimate bearing capacity. As part of the work, all graphical results from the laboratory model tests were provided to evaluate the normalized bearing pressure ($q/\gamma B$) and normalized settlement ratio (s/B), as detailed in the current investigation.

ACCEPTED MANUSCRIPT

The first group of tests was conducted on homogeneous UPt subgrade, aimed at comparing the performance of footings on uniform subgrade conditions. Fig. 8 illustrates the laboratory test results for unreinforced models, where the bearing pressure is plotted against settlement.

(Fig. 8 here)

Two separate tests were performed on different models prepared under the same conditions to ensure the repeatability of the results. The average of these two test results was used as the final outcome for the unreinforced model. Based on the data from Fig. 8, the ultimate bearing capacity for the unreinforced foundation was determined to be 74.63 kPa. It is important to note that the T0-01 test represents the unreinforced peat subgrade test in all scenarios, providing a benchmark for comparison.

C2. Unreinforced Layered Strata

As discussed in previous sections, a series of tests were conducted in succession. Subsequently, loading tests were performed on sand fill placed on the peat subgrade, compacted to the specified densities mentioned earlier, without the inclusion of reinforcement elements (T1 series). The T1 series involved tests on sand fills at varying densities, using two different embedment depths: H=2B and H=4B. The primary objective of these tests was to evaluate the effect of sand fill on the bearing capacity of the underlying peat subgrade. The sand fill was compacted to relative densities of 45% and 65%, and the corresponding graphs are shown in Fig. 9.

(Fig. 9 here)

Upon analyzing the experiments conducted within the T1 series, the ultimate bearing capacity values were determined to be 107.66 kPa for T1-2B-D45, 135.93 kPa for T1-2B-D65, 150.22 kPa for T1-4B-D45, and 186.36 kPa for T1-4B-D65. The results indicate a clear correlation, consistent with previous studies, where the ultimate bearing capacity increases as the relative density and H/B ratio are enhanced. Among the tests, the T1-2B-D45 produced the lowest ultimate bearing capacity, while the highest value was obtained in the T1-4B-D65 test. Compared to the T0 test, which recorded a bearing capacity of 74.63 kPa for the unreinforced peat subgrade, the IFs were calculated as 1.44, 1.82, 2.01, and 2.50, respectively. Clearly, as the H/B ratio increases, the bearing capacity behavior transitions from that of soft soils to a pattern more akin to that of granular soils. A similar effect is observed as the density of the sand fill on the peat subgrade increases.

C3. Reinforced Layered Strata

ACCEPTED MANUSCRIPT

C3.1 Investigating the effect of the top reinforcement layer embedment depth (u)

Prior to the tests, the ideal parameters for the model experiments were established through FEA. A total of seven u/B ratio values, ranging from 0.1 to 1.0, were assessed. The analysis of the FEA results showed that the u/B values of 0.2 and 0.3 provided the optimal outcomes. The experimental studies also considered different D_r and H/B depths, examining how these factors influenced the u/B ratio. A series of plate load tests (T2 series) were undertaken on sand reinforced with a single layer of geogrid in its planar form, at two embedment depth ratios, to investigate the impact of geogrid reinforcement on soil behavior. The results for N=1 is shown in Fig. 10, which depicts the variation in normalized bearing pressure and normalized settlement ratio for a footing resting on sand reinforced with geogrid at embedment depths of 0.2 and 0.3 times the width of the footing.

(Fig. 10 here)

The ultimate bearing capacities for the tests were 122.79 kPa for T2-2B-D45-u20 and 144.28 kPa for T2-2B-D45-u30. The calculated IF_0 values for these tests were 1.65 and 1.93, respectively. In the case of the unreinforced scenario (H=2B and D_r=45%), the ultimate bearing capacity was determined to be q_{1U}=107.66 kPa, which is known to serve as the reference value for IF_1. Consequently, the IF_1 values for T2-2B-D45-u20 and T2-2B-D45-u30 were 1.14 and 1.34, respectively. Table 10 consolidates the results for ultimate bearing capacities and all IF values, derived from different u/B ratios and the specified parameters H=2B, H=4B, Dr=45%, and Dr=65%. In Table 10, the test names in the "Test Info" section contain the indices "u20" and "u30," which represent u/B ratios of 0.20 and 0.30, respectively.

(Table 10 here)

As shown in Table 10, the IF_0 value reaches a maximum of 3.46, and the values for IF_1, IF_2, IF_3, and IF_4 are 1.34, 1.34, 1.28, and 1.39, respectively. These results are comparatively lower when compared to those reported in existing literature on sand reinforcement. The presence of UPt soil beneath the geogrid-reinforced sand is a key factor influencing the observed outcomes (Abu-Farsakh et al., 2013; Latha and Somwanshi, 2009; Useche-Infante et al., 2022).

The results clearly indicate that the inclusion of geogrid reinforcement improves the performance of the sand bed compared to the unreinforced scenario. The increase in strength is attributed to the frictional resistance developed between the geogrid and the sand, which prevents shearing at the reinforcement interface under vertical load conditions. Additionally, the confinement of the sand by the geogrid strips creates an interlocking effect that enhances the overall reinforcement process (Apurva et al., 2022). As the depth

ACCEPTED MANUSCRIPT

of the first reinforcement layer increases beyond 0.1B, a noticeable improvement in performance occurs, largely due to the higher frictional resistance generated at the sand-reinforcement interface, which is enhanced by the greater overburden pressure at deeper depths. However, when the depth exceeds 0.7B, an adverse effect on bearing capacity and settlement is observed, despite the settlement being lower than in the unreinforced case. This is due to the increased thickness of the sand layer above the reinforcement, which leads to higher settlements (Harikumar et al., 2020).

C3.2 Impact of vertical spacing (h) between reinforcement layers on bearing capacity

The depth of the first geogrid reinforcement layer was determined to be 0.2B and 0.3B, as previously discussed. For multi-layered reinforcement configurations, it is crucial to maintain optimal spacing between adjacent layers to maximize the overall capacity. The vertical spacing between the reinforcement layers was selected to be 0.2B and 0.3B. Fig. 11 presents the curves representing the relationship between normalized bearing pressure and normalized settlement ratio.

(Fig. 11 here)

On reviewing all the graphs presented in Fig. 11, it becomes clear that both the u/B ratio and the h/B ratio contribute to an increase in the ultimate bearing capacity as they are raised. The ultimate bearing capacities and IF values corresponding to all the experiments represented by the curves are presented in detail in Table 11. The indices 'h20' and 'h30' in the 'Test Info' column of Table 11 represent h/B ratios of 0.20 and 0.30, respectively.

(Table 11 here)

An analysis of Table 11 and Fig. 11 reveals that the values of IF_0, IF_1, IF_2, IF_3, and IF_4 reach up to 4.72, 1.92, 1.91, 1.92, and 1.89, respectively. Notably, when examining the reinforcement ratios of the different configurations of reinforced soil layers, it is observed that the IF values for these configurations are approximately similar. The IF values increased as the vertical spacing between the reinforcement layers increased. The maximum IF was observed at a vertical spacing ratio (h/B) of 0.3 for a settlement ratio (s/B) of 30%. When h is kept at 0.3B, it takes the maximum bearing pressure compared to other depths at the same settlement. An optimum amount of overburden pressure is required to mobilize the frictional resistance efficiently, as discussed in the previous section. Yetimoglu et al. suggested optimum spacing values of 0.2B and 0.4B for reinforced sands (Yetimoglu et al., 1994).

The experimental results indicate that the optimal reinforcement layer spacing for this geogrid material is h/B = 0.3, beyond which additional layers provide diminishing improvements in bearing capacity. This aligns with previous studies showing that stress

ACCEPTED MANUSCRIPT

distribution and reinforcement mobilization reach a plateau beyond a critical depth (Ahirwar and Mandal, 2021; Biswas, 2019). However, potential experimental constraints, such as scale effects, boundary conditions, and minor soil disturbance during sampling, may have influenced this threshold. In small-scale tests, geogrid stiffness is relatively higher, and lateral confinement may alter reinforcement efficiency compared to field conditions (Koerner, 2005; Zuo et al., 2021).

Approximately beyond s/B = 0.25, settlement stabilization is observed, primarily due to stress redistribution and tensile mobilization within the geogrid-reinforced system. As the footing penetrates deeper, geogrid layers resist further deformation, transitioning the system from plastic to a stabilized response. Additionally, the membrane effect enhances soil confinement, reducing incremental settlements. While this behavior aligns with previous studies experimental constraints such as scale effects and boundary conditions may have influenced the observed threshold. Small-scale models can overestimate geogrid stiffness, potentially leading to stabilization earlier than in full-scale conditions (Koerner, 2005). Furthermore, long-term consolidation and creep effects in field conditions could shift the stabilization point to a higher s/B ratio (Mesri and Ajlouni, 2007; Viswanadham and König, 2004). Despite these factors, similar trends have been observed in reinforced soils under varying conditions (Akbar et al., 2021; Mittal and Gill, 2018). Further validation through numerical modeling and large-scale field testing is necessary to refine these findings and assess their applicability in practical geotechnical design.

C3.3 Effect of the number of reinforcement layers (N)

The present research explores the reinforcement of sand fills using various configurations of reinforcement elements, with a particular focus on the number of elements as a key variable. Preliminary FEA simulations were performed to optimize the design parameters and understand the fills' behavior under different loading conditions. Building on the results of these simulations, loading tests were designed for configurations incorporating reinforcement element numbers of N=0 (unreinforced), N=1, and N=2. Specifically, the T2 and T3 test series utilized 1 and 2 geogrid elements, respectively, to evaluate the impact of reinforcement on the performance characteristics of the sand fill. The findings, presented in Fig. 12, illustrate how varying reinforcement element numbers influence the bearing capacity, particularly in relation to the H/B ratio and D_r, offering valuable insights into the effectiveness of reinforcement in enhancing fill performance.

(Fig. 12 here)

Upon analyzing Fig. 12, it is observed that increasing the number of geogrid elements results in an increase in bearing capacity, in line with existing literature. In tests conducted with u/B = 0.20 and D_r = 45%, under the condition of H=2B, a 14.1% increase in bearing capacity was observed with N=1, while a more significant increase of 38.4% was noted with N=2. The percentage changes in bearing capacity due to variations in the number of reinforcement elements across all experimental configurations are summarized

ACCEPTED MANUSCRIPT

in Table 12. In reviewing Table 12, it is essential to consider the variation in the number of reinforcement elements (N) within the context of the respective test group. Changes in parameters, such as the H/B ratio and D_r, may lead to inter-group comparisons, which could compromise the accuracy of interpretation by introducing inconsistencies due to differing test configurations. In light of this, the variations in the bearing capacity values presented in this table were calculated by comparing them to the bearing capacity values of the unreinforced condition within the corresponding group. This methodology ensures that the effect of reinforcement is assessed to baseline conditions, thus providing a more comprehensive understanding of the reinforcement's contribution to the overall performance.

(Table 12 here)

An analysis of the test results presented in Table 12 demonstrates a notable increase in bearing capacity compared to the unreinforced condition under D_r=45% and N=1. The observed increase in bearing capacity ranges from 22.8% to 24.1%. Similarly, for D_r=65% and N=1, the bearing capacity increases within the range of 24.8% to 28.7%. Under the N=2 condition, the average change in bearing capacity indicates that, for D_r=45%, the relative density values range from 66.2% to 67.1%. When D_r is increased to 65%, the relative density values correspondingly rise to a range of 71.8% to 72.7%. When examining the changes in bearing capacity under identical H/B ratios, it is observed that the variation in relative density values has a negligible effect on bearing capacity under the D_r=45% and N=1 conditions. A similar conclusion can be drawn for N=2, where no significant variation in bearing capacity is observed. However, at D_r=65% and N=2, the average changes in bearing capacity remain relatively consistent across both H/B ratios. In contrast, for N=1, a more pronounced improvement in bearing capacity is evident when the H/B ratio is 4B.

C3.4 Effect of fill depth (H)

In the context of soil reinforcement studies, two distinct H/B ratios were examined through preliminary FEA. Initially, nine different ratios, ranging from H/B = 0.5 to 7.0, were subjected to preliminary analysis. Based on the results, bearing capacity values for these various H/B ratios were evaluated, leading to the selection of H = 2.0B and H = 4.0B for further investigation. The preliminary analysis results revealed that, at an H/B ratio of 2.0, the influence of the undisturbed peat soil beneath the sand fill was still evident. In contrast, at H/B = 4.0, the system exhibited behavior more akin to that of sand soil under axial load. Additionally, it was determined that bearing capacity values at H/B ratios of 5.0, 6.0, and 7.0 were nearly identical to those at H/B = 4.0. Given its engineering feasibility, cost-effectiveness, and broader applicability, the H/B = 4.0 ratio was selected for subsequent analysis.

ACCEPTED MANUSCRIPT

Based on the bearing capacity values presented for different configurations in Table 12, the following conclusions can be drawn:

- Under the conditions of N=0 and D_r=45%, a 44.3% increase in bearing capacity was observed for the H/B = 2.0 ratio compared to the unreinforced peat soil condition. For the H/B = 4.0 ratio, the bearing capacity increased by 101.3% relative to the unreinforced peat soil. Similarly, under the conditions of N=0 and D_r=65%, the bearing capacity at H/B = 2.0 increased by 82.1% compared to the unreinforced peat soil, while for H/B = 4.0, the increase in bearing capacity was 149.7%.
- For the N=1 condition with D_r=45%:

  At H/B = 2.0 and u/B = 0.2, a 14.1% increase in bearing capacity was observed compared to the unreinforced sand fill condition. For the u/B = 0.30 condition, the increase was 34.0%. At H/B = 4.0 and u/B = 0.2, a 14.2% increase in bearing capacity was noted, whereas at H/B = 4.0 and u/B = 0.3, the increase was 28.3%.
- For the N=1 condition with D_r=65%:

  At H/B = 2.0 and u/B = 0.2, the bearing capacity exhibited an increase of 15.8% compared to the unreinforced sand fill condition, whereas at u/B = 0.30, the increase was 33.7%. At H/B = 4.0 and u/B = 0.2, the bearing capacity showed an increase of 18.7%, and at H/B = 4.0 and u/B = 0.3, the increase was observed to be 38.6%.

Considering all the tests and preliminary analyses conducted, the increase in the H/B ratio from 2.0 to 4.0 has resulted in a corresponding increase in bearing capacity values.

C3.5 Percentage reduction in settlement

The enhancement of foundation bed performance through geogrid reinforcement can be effectively quantified by evaluating the reduction in footing settlement. This is commonly expressed using the Percentage Reduction in Settlement (PRS), a parameter that indicates the degree to which planar reinforcement mitigates settlement under applied loads. The PRS is mathematically defined by the equation provided in the 'Test Variables' section of this paper.

Given that the performance improvement is evaluated relative to the unreinforced sand, and previous research from various small-scale model tests suggests that the ultimate bearing capacity of unreinforced soil is reached at a settlement of 5–10% of the foundation width, the ultimate bearing capacity in the current study was defined at a settlement corresponding to 10% of the footing width (s/B = 10%) (Doley et al., 2021). The settlement of the reinforced foundation bed at this load, denoted as S_r, represents the settlement under the ultimate bearing pressure of an unreinforced foundation bed. Fig. 13 presents the PRS values for different reinforcement types and combinations, calculated at s/B = 0.10 from experiments conducted under varying densities and H/B ratios.

(Fig. 13 here)

ACCEPTED MANUSCRIPT

The highest PRS of 79% (for 4B-D65-u30-h30) was observed for a sand bed reinforced with geogrids. This PRS value indicates a 79% reduction in settlement in the reinforced sand bed compared to the unreinforced sand bed. The significant reduction in settlement can be attributed to the beam action of the geogrids, which distribute the applied load over a wider area. This redistribution reduces the intensity of pressure on the underlying soil, resulting in lower settlement. Additionally, the inclusion of a basal geogrid further mitigates settlement by restricting the downward movement of the soil. These results align with previous findings reported by Hegde and Sitharam (Hegde and Sitharam, 2015).

C3.6 Surface heaving behavior

Previous research has shown that the maximum heave typically occurs at a distance of 1.5B from the center of the footing (Dash et al., 2004; Latha and Somwanshi, 2009). Accordingly, in the present study, dial gauges for measuring heave were positioned at distances of 1.5B and 2.5B from the center of the footing, and the corresponding surface deformations (heave/settlement) were recorded as described by Lal et al. (Lal et al., 2017). Additionally, it has been established that the surface deformation of unreinforced soil extends from the center of the foundation to a distance of 2.5B, with the maximum deformation generally occurring at approximately 1.5B. In this context, positive deformation is defined as the settlement of the footing, while negative deformation corresponds to the heave of the subgrade surface.

The surface deformation depends on footing settlement. The variation in surface settlement on the left and right sides of the footing is a result of the footing's tilting, a phenomenon commonly observed in small-scale laboratory experiments (Biswas et al., 2022). The surface heaving was observed maximum for the unreinforced system at the distance of 1.5B for T0-01. For all experimental configurations, surface heaving values have been determined, and the outcomes for the unreinforced peat and sand fill are provided in Fig. 14.

(Fig. 14 here)

Heaving was also observed in the case of fill beds reinforced with geogrid; however, the magnitude of heaving was reduced compared to that of the unreinforced fill bed. When the fill bed was reinforced with geogrid, surface heaving was completely mitigated, and instead, settlement of the fill was observed. The maximum settlement of the fill, up to 4.4% of the footing width, was recorded in the case of geogrid-reinforced fill beds. Furthermore, the settlement was reduced when additional geogrid layers were placed at different depths. The minimum settlement was observed in the case of two-layer geogrid reinforcement (N=2), with minimal difference in settlement between N=1 and N=2. Hegde and Sitharam noted that the provision of multiple geogrid layers

ACCEPTED MANUSCRIPT

leads to a significant reduction in surface heave (Hegde and Sitharam, 2015). In the lower settlement range, the foundation bed behaves like a rigid body, with the inclusion of geogrid reinforcement resulting in increased surface settlements (Latha and Somwanshi, 2009).

Surface heave reduction in geogrid-reinforced systems results from a combination of lateral restraint and vertical confinement, with further optimization possible through adjustments in tensile strength, aperture size, and material properties. Higher tensile strength enhances lateral restraint, reducing heave, but excessive stiffness may cause over-confinement, limiting effectiveness (Hegde and Sitharam, 2015; Makkar et al., 2016). Aperture size plays a crucial role in soil interlocking, preventing lateral spreading while maintaining flexibility (Abdi and Etefagh, 2014; Mehrjardi and Khazaei, 2017).

C3.7 Geogrid deformation

The research involved preparing different configurations of sand fill over undisturbed large-scale peat subgrade soils. The sand fills were tested both in an unreinforced condition and with geogrid reinforcement. Following each test with geogrid reinforcement, the area around the geogrid was carefully excavated to the depth of the geogrid layer. Displacement values of the geogrid element, induced by axial loading, were measured at these depths. This procedure was consistently applied across all experiments involving geogrid reinforcement. The observed geogrid displacements after testing are shown in Fig. 15, which presents visual representations of the displacement values for four different tests. These selected test cases were chosen to represent varying densities and H/B ratios.

(Fig. 15 here)

Displacement values of geogrid elements measured in reinforced sand fill soils for different geogrid configurations (N=1 and N=2) are presented in Table 13.

(Table 13 here)

In all conducted tests, both with and without reinforcement, the loading procedure was applied up to a value of 5B (40 mm). According to the data presented in Table 13, deformation values of the geogrid elements were recorded in all cases where reinforcement was provided. The authors introduced a new parameter, the Displacement Accommodation Ratio (DAR), which is defined as the ratio of the deformation measured in the geogrid element ($\delta_{geogrid}$) to the final displacement observed in the footing ($s_{footing}$) during the test. This relationship is formalized in Equation 5. It is important to highlight that, for the tests with N = 2, N1

ACCEPTED MANUSCRIPT

refers to the geogrid element located at the upper reinforcement layer, while N2 represents the geogrid element at the lower reinforcement layer.

$$\text{DAR}\,[\%] = \left(\frac{\delta_{\text{geogrid}}}{s_{\text{footing}}} \right) \times 100 \tag{5}$$

The deformation values of the geogrid elements, as shown in Table 13, were analyzed for various test conditions. For the N = 1 case, the maximum geogrid deformation of s = 34.0 mm occurred in the T2-4B-D65-u20 test, while the minimum deformation of s = 24.0 mm was observed in the T2-2B-D65-u30 test. It was found that, for a constant H/B ratio, an increase in relative density resulted in an increase in geogrid deformation. Similarly, for a fixed relative density, an increase in the H/B ratio also caused the geogrid deformation to rise. In contrast, an increase in the u/B ratio from 0.20 to 0.30 led to a decrease in deformation.

For the N = 2 condition, the deformation values measured under both H/B = 2.0 and H/B = 4.0 conditions indicated that as the relative density of the sand increased, the deformation values of both the upper (N1) and lower (N2) geogrid elements decreased. At D_r=45%, when the H/B ratio increased from 2.0 to 4.0, deformation values for both N1 and N2 elements increased. Similarly, at D_r=65%, an increase in the H/B ratio from 2.0 to 4.0 led to an increase in deformation for the N1 element. However, a different trend was observed for the N2 element. Specifically, in the T3-2B-D65-u20-h20 test, the deformation value for the N1 element decreased, while the deformation of the N2 element showed a reduction, exhibiting contrasting behavior compared to the N1 element. An analysis of the DAR ratio for the N = 1 condition shows that the highest deformation accommodation ratio, 85.0%, was recorded in the T2-4B-D65-u20 test. The lowest DAR ratio for this condition was found in the T2-2B-D45-u30 test. For the N = 2 condition, the upper N1 element exhibited the highest DAR ratio of 70.0% in the T3-4B-D45-u20-h20 test, while the lowest DAR ratio, 42.5%, was observed in the T3-2B-D45-u30-h30 and T3-2B-D65-u30-h30 tests.

D. Conclusions

This study investigates the impact of geogrid reinforcement on the bearing capacity and settlement behavior of footings placed on peat subgrade with varying fill densities (D_r) and H/B ratios. The findings provide valuable insights into the design of geogrid-reinforced foundations, particularly on peat soils, contributing to the optimization of load distribution and reduction of settlement.

A key aspect of this paper is the use of undisturbed peat samples, ensuring more accurate and realistic results compared to disturbed samples. This approach captures the true in-situ properties of peat, critical for understanding foundation behavior in real-world conditions. Consolidation tests confirmed minimal disturbance, classifying the peat as 'very good to excellent' quality, enhancing the novelty of the study and bridging the gap between laboratory and real-world performance.

- The T0 test (unreinforced peat subgrade) resulted in an ultimate bearing capacity of 74.63 kPa, serving as the baseline for comparison in subsequent tests. The T1 test results show a significant improvement in bearing capacity with geogrid reinforcement. The maximum bearing capacity was observed in the T1-4B-D65 test, where a 150% increase was

ACCEPTED MANUSCRIPT

recorded, resulting in 186.36 kPa. In contrast, the minimum bearing capacity was observed in the T1-2B-D45 test, showing a 44.3% increase with a value of 107.66 kPa. These findings highlight the effectiveness of geogrid reinforcement, with higher fill densities and H/B ratios yielding the most significant improvements in bearing capacity.

- The T2 test results show significant improvements in bearing capacity with geogrid reinforcement. The maximum bearing capacity was observed in the T2-4B-D65-u30 test, reaching 258.26 kPa, corresponding to a 245.5% increase compared to the unreinforced T0 condition. The minimum bearing capacity was recorded in the T2-2B-D45-u20 test at 122.79 kPa, showing a 64.6% increase compared to T0. The T3 test results exhibited notable improvements in bearing capacity with the addition of geogrid reinforcement. The maximum bearing capacity was observed in the T3-4B-D65-u30-h30 test, where a value of 352.16 kPa was recorded, corresponding to a 372.5% increase compared to the unreinforced T0 condition. The minimum bearing capacity was observed in the T3-2B-D45-u20-h20 test, with a value of 148.99 kPa, showing a 100.2% increase compared to T0.
- The results indicate a significant reduction in settlement with geogrid reinforcement. The maximum settlement reduction was observed in the T3-4B-D65-u30-h30 test, with a 79% reduction compared to the unreinforced T0 condition.
- Geogrid reinforcement significantly reduced surface heaving compared to unreinforced fill beds. In geogrid-reinforced fill beds, surface heaving was completely mitigated, and settlement was observed instead, with a maximum settlement of 4.4% of the footing width. The addition of multiple geogrid layers further reduced settlement, with minimal difference between single and double-layer configurations (N=1 and N=2).
- For N=1, the maximum geogrid deformation was observed in the T2-4B-D65-u20 test with 34.0 mm of deformation. For N=2, the maximum geogrid deformation was observed in the T3-4B-D45-u20-h20 test with 28.0 mm (N2) of deformation. These results highlight the significant influence of geogrid layers on deformation, with multi-layer configurations reducing deformation compared to single-layer configurations.

This study provides valuable experimental data from laboratory-scale tests on undisturbed peat; however, field variations remain unaccounted for. Future research should assess the long-term performance of geogrid-reinforced foundations under cyclic loading and varying environmental conditions. These findings have practical implications for foundation design in peat areas, where geogrid reinforcement can enhance performance, reduce settlement, and lower maintenance costs.

While increasing relative density enhances bearing capacity, achieving 65% in field conditions may be challenging due to equipment constraints and potential soil disturbance. Alternative approaches, such as optimized geogrid placement, geotextiles, lightweight fill, and chemical stabilization, provide practical solutions for improving performance at lower densities. Future research should emphasize large-scale field validation, numerical modeling, and the long-term effectiveness of these methods to develop more efficient strategies for stabilizing peat subgrades and bridging the gap between laboratory findings and real-world applications.

ACCEPTED MANUSCRIPT

Our results indicate that optimizing geogrid placement depth and layer spacing is often more effective in enhancing reinforcement performance than merely increasing tensile strength. Future research will further investigate the influence of reinforcement configurations and explore alternative material properties to maximize improvement factors.

A key area for future research is the numerical modeling of geogrid-reinforced systems, which would provide a more detailed understanding of load transfer, stress distribution, and deformation behavior. Techniques such as Finite Element Modeling (FEM) and Discrete Element Modeling (DEM) can help simulate the interaction between geogrid and soil under different loading conditions, improving predictions of reinforcement effectiveness and foundation stability.

Additionally, the impact of dynamic loading on reinforced peat foundations, particularly in applications like road embankments and railways, should be investigated. Understanding the behavior of geogrid-reinforced foundations under cyclic loading conditions will provide insights into the durability and performance of these foundations under repeated stress.

Credit Author Statement

Both authors contributed equally to the conceptualization of the research problem and its objectives. The model tests and research investigation were carried out by the first author, with technical guidance and input from the second author. Both authors collaborated in writing and finalizing the manuscript.

Data Availability Statement

All data, models, and code generated or used during the study appear in the submitted manuscript. Some or all data, models, or codes that support the findings of this research are available from the corresponding author upon reasonable request.

Declarations

Competing of interest: The authors declare that they have no known competing financial interests or personal relationships that could have appeared to influence the work reported in this research.

Acknowledgments

The authors are thankful to the Kayseri Free Zone Administration for providing the site necessary for this research, and to İstanbul Teknik Geoteknik for their support in supplying the geogrid elements.

Funding

No financial support was provided for this research from any public, commercial, or non-profit funding agencies.

ACCEPTED MANUSCRIPT

References

Abdi, M., Etefagh, M., 2014. The Effect of Soil Particle Size and Reinforcement Aperture Size on the Soil–Geogrid Interaction. Experimental Research in Civil Engineering 1, 57-64.

Abu-Farsakh, M., Chen, Q.M., Sharma, R., 2013. An experimental evaluation of the behavior of footings on geosynthetic-reinforced sand. Soils Found 53, 335-348.

Adili, A.A., Azzam, R., Spagnoli, G., Schrader, J., 2012. Strength of soil reinforced with fiber materials (Papyrus). Soil Mech Found Eng+ 48, 241-247.

Ahirwar, S.K., Mandal, J.N., 2021. Behaviour of bamboo grid-reinforced soil bed. Int J Geotech Eng 15, 867-876.

Ahmad, H., 2022. Sustainability effect of geogrid reinforced tire-shred sand mixtures on the load pressure-settlement response of shallow footing. Heliyon 8, e11743.

Akbar, A., Bhat, J.A., Mir, B.A., 2021. Plate load tests for investigation of the load-settlement behaviour of shallow foundation on bitumen-coated geogrid reinforced soil bed. Innov Infrastruct So 6.

Akhil, K.S., Sankar, N., Chandrakaran, S., 2022. Effect of Aperture Size on the Performance of Bamboo Mat Reinforced Soil Bed. J Nat Fibers 19, 6909-6920.

Al-Barqawi, M., Aqel, R., Wayne, M., Titi, H., Elhajjar, R., 2021. Polymer Geogrids: A Review of Material, Design and Structure Relationships. Materials 14.

Al-Haddad, S.A., Al-Ani, F.H., Fattah, M.Y., 2022. Effect of Using Plastic Waste Bottles on Soil Response above Buried Pipes under Static Loads. Appl Sci-Basel 12.

Alawaji, H.A., 2001. Settlement and bearing capacity of geogrid reinforced sand over collapsible soil. Geotext Geomembranes 19, 75-88.

Aminu, I., Asadi, A., O'Kelly, B.C., Huat, B.B.K., Reul, O., 2022. Ultralightweight foundation system for peaty ground. Environ Geotech-J 9, 12-21.

Amundsen, H.A., Thakur, V., Emdal, A., 2016. Sample disturbance in blocksamples of low plastic soft clays, In Proceedings of the 17th Nordic Geotechnical Meeting Challenges in Nordic Geotechnics, pp. 159-168.

Andresen, A., Kolstad, P., 1979. The NGI 54 mm samplers for undisturbedsampling of clays and representative sampling of coarser materials, In Pro-ceedings of the International Symposium on Soil Sampling, pp. 13-21.

Apurva, A.K., Chandrakaran, S., Sankar, N., 2022. Effectiveness of using rattan fiber as a soil-reinforcing material and its application in different forms. Int J Environ Sci Te.

Asakereh, A., Ghazavi, M., MoghaddasTafreshi, S.N., 2013. Cyclic response of footing on geogrid-reinforced sand with void. Soils Found 53, 363-374.

ASTM, 1992. D4427-92 Standard classification of peat samples by laboratory testing. ASTM International, West Conshohocken, US.

ASTM, 2000. D1587-00 Standard Practice for Thin-Walled Tube Sampling of Soils for Geotechnical Purposes. American Society for Testing and Materials International.

ASTM, 2012. D1196/D1196M Nonrepetitive Static Plate Load Tests of Soils and Flexible Pavement Components, for Use in Evaluation and Design of Airport and Highway Pavements. American Society for Testing and Materials International.

ASTM, 2020. D2435 Standard test methods for onedimensional consolidation properties of soils using incremental loading. American Society for Testing and Materials International.

Azzam, W.R., Nasr, A.M., 2014. Bearing capacity of shell strip footing on reinforced sand. Journal of Advanced Research 6, 727-737.

Basudhar, P.K., Saha Roy, S., Deb, K., 2007. Circular footings resting on geotextile-reinforced sand bed. Geotext Geomembranes 25, 377-384.

Bathurst, R.J., Naftchali, F.M., 2021. Geosynthetic reinforcement stiffness for analytical and numerical modelling of reinforced soil structures. Geotext Geomembranes 49, 921-940.

Bhardwaj, A., Sharma, R.K., 2023. Experimental and Numerical Investigations on the Bearing Capacity of Footings on the Layered Soil. Int J Geosynth Groun 9.

Biswas, A., 2019. Comparative performance of different geosynthetics on sandy soil overlying clay subgrades of varying strengths. Innov Infrastruct So 4.

ACCEPTED MANUSCRIPT

Biswas, S., Hussain, M., Singh, K.L., 2022. Performance Evaluation of Infill Materials of Geocell-Reinforced Granular Bed Overlying Soft Subgrade. Indian Geotech J.

Bowles, J., 1997. Foundation analysis and design. McGraw-Hill, New York.

Buragadda, V., Thyagaraj, T., 2019. Bearing Capacity of Jute Geotextile-Reinforced Sand Bed. Int J Geosynth Groun 5.

Cerato, A., Lutenegger, A., 2007. Scale Effects of Shallow Foundation Bearing Capacity on Granular Material. J. Geotech. Geoenviron. Eng 133, 1192-1202.

Chenari, M.J., Payan, M., Chenari, R.J., Dastpak, P., Sousa, R.L., 2023. Probabilistic Assessment of Bearing Capacity of Strip Footings Seated on Geosynthetic Reinforced Soil Deposits Using Finite Element Limit Analysis (FELA) and Response Surface Method (RSM). Geo-Congress 2023: Geotechnical Data Analysis and Computation 342, 40-50.

Chmielewska, I., 2023. Effect of fibre content on the geotechnical properties of peat. Stud Geotech Mech.

Çadır, C.C., Kaya, Z., Yalcin, H., Erol, A., Uncuoğlu, E., Akin, M., 2024. Experimental Investigation of Soil Disturbance Effect on Bearing Capacity of Organic Soil. International Journal of Civil Engineering 22, 225-240.

Das, B.M., 2013. Principles of Foundation Engineering, 8th ed. ed. Cengage Learning.

Das, B.M., Omar, M.T., 1994. The effects of foundation width on model tests for the bearing capacity of sand with geogrid reinforcement. Geotechnical & Geological Engineering 12, 133-141.

Dash, S.K., Rajagopal, K., Krishnaswamy, N.R., 2004. Performance of different geosynthetic reinforcement materials in sand foundations. Geosynth Int 11, 35-42.

Demir, A., Laman, M., Yildiz, A., Ornek, M., 2013. Large scale field tests on geogrid-reinforced granular fill underlain by clay soil. Geotext Geomembranes 38, 1-15.

Derksen, J., Fuentes, R., Ziegler, M., 2022. Geogrid-soil interaction: experimental analysis of factors influencing load transfer. Geosynth Int.

Doley, C., Das, U.K., Shukla, S.K., 2021. Response of Square Footing on Geocell-Reinforced Sand Bed Under Static and Repeated Loads. Int J Geosynth Groun 7.

El-Sawwaf, M., Nazir, A.K., 2010. Behavior of repeatedly loaded rectangular footings resting on reinforced sand. Alexandria Engineering Journal 49, 349-356.

El Sawwaf, M.A., Nazir, A., 2012. Behavior of eccentrically loaded small-scale ring footings resting on reinforced layered soil. J Geotech Geoenviron 138, 376-384.

El Wakil, A.Z., 2010. Horizontal capacity of skirted circular shallow footings on sand. Alexandria Engineering Journal 49, 379-385.

Fatehi, M., Yaghoobi, B., Payan, M., Hosseinpour, I., Chenari, R.J., 2023. Combined bearing capacity of footings on geogrid-reinforced granular fill over soft clay. Geosynth Int 31, 942-967.

Fathipour, H., Payan, M., 2023. Seismic Bearing Capacity of Eccentrically and Obliquely Loaded Strip Footings on Geosynthetic-Reinforced Soil. Int J Geomech 23.

Gedela, R., Karpurapu, R., 2021. Laboratory and Numerical Studies on the Performance of Geocell Reinforced Base Layer Overlying Soft Subgrade. Int J Geosynth Groun 7.

Ghadr, S., Assadi-Langroudi, A., 2022. Stabilisation of peat with colloidal nano and micro silica. Mires Peat 28.

Ghosh, A., Ghosh, A., Bera, A.K., 2005. Bearing capacity of square footing on pond ash reinforced with jute-geotextile. Geotext Geomembranes 23, 144-173.

Guido, V.A., Chang, D.K., Sweeney, M.A., 1986. Comparison of geogrid and geotextile reinforced earth slabs. Can Geotech J 23, 435-440.

Guo, X.P., Zhang, H., Liu, L.L., 2020. Planar geosynthetic-reinforced soil foundations: a review. Sn Appl Sci 2.

Hajj, A.R., 1990. The simulation of sampling disturbance and its effectson the deformation behaviour of clays. University of Sheffield.

Hamed, M., Emirler, B., Canakci, H., Yildiz, A., 2020. 3D Numerical Modeling of a Single Pipe Pile Under Axial Compression Embedded in Organic Soil. Geotech Geol Eng 38, 4423-4434.

Harikumar, M., Sankar, N., Chandrakaran, S., 2016. Behaviour of model footing resting on sand bed reinforced with multi-directional reinforcing elements. Geotext Geomembranes 44, 568-578.

Harikumar, M., Sankar, N., Chandrakaran, S., 2020. Effect of Multi-Directional Reinforcements on the Settlement and Heave Characterstics of Foundations on Sand. Geotech Geol Eng.

ACCEPTED MANUSCRIPT

Hegde, A., Sitharam, T.G., 2015. Use of Bamboo in Soft-Ground Engineering and Its Performance Comparison with Geosynthetics: Experimental Studies. J Mater Civil Eng 27.

Hejazi, S.M., Sheikhzadeh, M., Abtahi, S.M., Zadhoush, A., 2012. A simple review of soil reinforcement by using natural and synthetic fibers. Constr Build Mater 30, 100-116.

Holtz, R.D., Kovacs, W.D., Sheahan, T.C., 2011. An Introduction to Geotechnical Engineering, 2nd ed. Pearson.

Hosseini, M., Yaghoobi, B., Ranjbar, P.Z., Payan, M., Chenari, R.J., 2023. Stability Analysis of Geosynthetic-Reinforced Shallow Foundations with a Lower-Bound FELA Approach Adopting the Nonassociated Plastic Flow Rule. Int J Geomech 23.

Huat, B.B., Kazemian, S., Prasad, A., Barghchi, M., 2011. A study of the compressibility behavior of peat stabilized by DMM: Lab Model and FE analysis. Scientific Research and Essays 6, 196-204.

Indraratna, B., Bamunawita, C., Khabbaz, H., 2012. Numerical modeling of soft ground stabilized with vertical drains and vacuum preloading. Can Geotech J 39, 1-18.

ISO, 2024. ISO 10319:2024 Geosynthetics - Wide-width tensile test. International Organization for Standardization.

Jong-Seok, L., 2004. An Experimental investigation of Boussinesq's theoretical value of vertical stress increment in sandy soil mass caused by surface strip loading. Journal of the Korean Geotechnical Society 20, 5-15.

Juneja, G., Sharma, R.K., 2023. Experimental and Numerical Analysis of Geocell-Reinforced Base Layer with Different Infill Materials Overlying Clay. Journal of Hazardous, Toxic, and Radioactive Waste 27.

Kalyan, K., Krishna, V.R., 2021. Analytical study on failure of granular anchor pile. Mater Today-Proc 46, 8393-8396.

Kargar, M., Hosseini, S.M.M.M., 2017. Effect of reinforcement geometry on the performance of a reduced-scale strip footing model supported on geocell-reinforced sand. Sci Iran 24, 96-109.

Karlsrud, K., Hernandez-Martinez, F.G., 2013. Strength and deformation properties of Norwegian clays from laboratory tests on high-quality block samples. Can Geotech J 50, 1273-1293.

Kaya, Z., Erol, A., 2021. Comparison of bearing capacities of undisturbed organic soils by empirical relations and 2D finite element analysis. Arabian Journal of Geosciences 14, 1975.

Keskin, M.S., Bildik, S., Laman, M., 2023. Experimental and Numerical Studies of Vertical Stresses Beneath the Circular Footings on Sand. Applied Sciences 13, 1635.

Koerner, R.M., 2005. Designing with Geosynthetics, Fifth Edition ed. Prentice Hall, New Jersey.

Krishna, A.M., Biswas, A., 2021. Performance of Geosynthetic Reinforced Shallow Foundations. Indian Geotech J 51, 583-597.

Kumar, J., Khatri, V.N., 2008. Effect of footing width on Nγ. Can Geotech J 45, 1673-1684.

Kuranchie, F.A., Shukla, S.K., Habibi, D., Kazi, M., 2016. Load–settlement behaviour of a strip footing resting on iron ore tailings as a structural fill. International Journal of Mining Science and Technology 26, 247-253.

Kusakabe, O., 1995. Chapter 6 of Geotechnical Centrifuge Technology, in: Taylor, R.N. (Ed.), Foundations. Blackie Academic and Professional, London.

Lade, P., Lee, K.L., 1976. Engineering properties of soils. University of California, Los Angeles, California.

Lal, D., Sankar, N., Chandrakaran, S., 2017. Behaviour of square footing on sand reinforced with coir geocell. Arab J Geosci 10.

Langhaar, H.L., 1951. Dimensional analysis and theory of models. Wiley, New York.

Latha, G.M., Somwanshi, A., 2009. Bearing capacity of square footings on geosynthetic reinforced sand. Geotext Geomembranes 27, 281-294.

Latha, G.M., Somwanshi, A., Reddy, K.H., 2013. A Multiple Regression Equation for Prediction of Bearing Capacity of Geosynthetic Reinforced Sand Beds. Indian Geotech J 43, 331-343.

Li-Hua, L., Shuai-Shuai, L., Heng-Lin, X., Wei-Qiang, F., Jun-Peng, L., Pei-Chen, W., 2022. Experimental investigation on reinforcement effect of sustainable materials for different subgrades. J Clean Prod 343.

Liu, C.N., Yang, K.H., Nguyen, M.D., 2014. Behavior of geogrid–reinforced sand and effect of reinforcement anchorage in large-scale plane strain compression. Geotext Geomembranes 42, 479-493.

Long, M., 2005. Review of peat strength, peat characterisation and constitutive modelling of peat with reference to landsides. Stud Geotech Mech 27, 67-90.

Madani, N., Hosseinpour, I., Payan, M., Senetakis, K., 2023. Cyclic and Postcyclic Interface Characteristics of Geotextile-Embedded Sand-Rubber Composites. J Mater Civil Eng 35.

Makkar, F.M., Chandrakaran, S., Sankar, N., 2016. Settlement and surface heave characteristics of geogrid reinforced cohesionless soil, Indian geotechnical conference IGC2016.

ACCEPTED MANUSCRIPT

Mayne, P.W., Christopher, B.R., DeJong, J.T., 2002. Subsurface Investigations: Geotechnical Site Characterization. Federal Highway Administration (FHWA).

Mehrjardi, G.T., Khazaei, M., 2017. Scale effect on the behaviour of geogrid-reinforced soil under repeated loads. Geotext Geomembranes 45, 603-615.

Merse, M.M., Hosseinpour, I., Payan, M., Chenari, R.J., Mohapatra, S.R., 2023. Shear Strength Behavior of Soft Clay Reinforced with Ordinary and Geotextile-Encased Granular Columns. Int J Geosynth Groun 9.

Mesri, G., Ajlouni, M., 2007. Engineering properties of fibrous peats. J Geotech Geoenviron 133, 850-866.

Mittal, A., Shukla, S., 2018. Influence of geotextile and geogrid reinforcement on strength behaviour of soft silty soil. Applied Mechanics and Materials 877, 264-269.

Mittal, R.K., Gill, G., 2018. Sustainable application of waste tire chips and geogrid for improving load carrying capacity of granular soils. J Clean Prod 200, 542-551.

Mittal, R.K., Gill, G., 2020. Pressure settlement behaviour of strip footing resting on tire-chip reinforced sand. Int J Geotech Eng 14, 162-168.

Moghaddas Tafreshi, S.N., Khalaj, O., Halvaee, M., 2011. Experimental study of a shallow strip footing on geogrid-reinforced sand bed above a void. Geosynth Int 18, 178-195.

Nagaraj, T.S., Murthy, B.S., Vatsala, A., Joshi, R.C., 1990. Analysis of compressibility of sensitive soils. Journal of Geotechnical Engineering 116, 105-118.

Neto, J.O.A., Bueno, B.S., Futai, M.M., 2013. A bearing capacity calculation method for soil reinforced with a geocell. Geosynth Int 20, 129-142.

NGF, 2012. Veiledning for Grunnforsterkning med Kalksementpeler. Norsk geoteknisk forening, Oslo, Norway.

Norazam, P.N.F.I., Bakar, I., Siang, A.J.L.M., Herman, H.S., 2017. Stabilization of Peat Soil by Using Envirotac. International Symposium on Civil and Environmental Engineering 2016 (Iscee 2016) 103.

Okamura, M., Mihara, A., Takemura, J., Kuwano, J., 2002. Effects of Footing Size and Aspect Ratio on the Bearing Capacity of Sand Subjected to Eccentric Loading. Soils Found 42, 43-56.

Omar, M.T., Das, B.M., Puri, V.K., Yen, S.C., 1993. Ultimate bearing capacity of shallow foundations on sand with geogrid reinforcement. Can Geotech J 30, 545-549.

Ovesen, N.K., 1979. The scaling low relationship-Panel discussion, Proc. 7th European Regional Conf. on SMFE, pp. 319-323.

Özer, M., 2021. Determination of the relationship between geogrid aperture size and aggregate particle size. Arab J Geosci 14, 3.

Panagiotidou, A.I., 2010. 2D and 3D inelastic seismic response analysis of foundation with uplifting and P–Δ effects. National Technical University, Athens, Greece.

Park, J.B., Park, H.S., Kim, D., 2013. Geosynthetic Reinforcement of Sand-Mat Layer above Soft Ground. Materials 6, 5314-5334.

Peng, B., Feng, R., Wu, L., Wei, K., Wang, P., 2023. Settlement calculation method for peat soil foundations. Int J Geomech 23, 04023094.

Prakash K, K., Rathod, D., Muthukkumaran, K., 2023. Role of Geogrid reinforcement and its diverse applications in the geotechnical engineering and allied fields: a-state-of-the-art review. Australian Journal of Civil Engineering, 1-19.

Razali, S.N.M., Bakar, I., Zainorabidin, A., 2013. Behaviour of Peat Soil in Instrumented Physical Model Studies. Procedia Engineer 53, 145-155.

Rezanezhad, F., Price, J.S., Quinton, W.L., Lennartz, B., Milojevic, T., Van Cappellen, P., 2016. Structure of peat soils and implications for water storage, flow and solute transport: A review update for geochemists. Chemical Geology 429, 75-84.

Rikmann, E., Zekker, I., Teppand, T., Pallav, V., Shanskiy, M., Maeorg, U., Tenno, T., Burlakovs, J., Liiv, J., 2021. Relationship between Phase Composition and Mechanical Properties of Peat Soils Stabilized Using Oil Shale Ash and Pozzolanic Additive. Water-Sui 13.

Roy, S.S., Deb, K., 2017. Effects of aspect ratio of footings on bearing capacity for geogrid-reinforced sand over soft soil. Geosynth Int 24, 362-382.

Saberian, M., Rahgozar, M.A., 2016. Geotechnical properties of peat soil stabilised with shredded waste tyre chips in combination with gypsum, lime or cement. Mires Peat 18.

Salamatpoor, S., Jafarian, Y., Hajiannia, A., 2018. Bearing Capacity and Uneven Settlement of Consecutively Constructed Adjacent Footings Rested on Saturated Sand Using Model Tests. International Journal of Civil Engineering 17, 737-749.

Shadmand, A., Ghazavi, M., Ganjian, N., 2018. Load-settlement characteristics of large-scale square footing on sand reinforced with opening geocell reinforcement. Geotext Geomembranes 46, 319-326.

ACCEPTED MANUSCRIPT

Shafiee, A., Fathipour, H., Payan, M., Jalili, J., Chenari, R.J., 2024. Modulus reduction and damping characteristics of geotextile-reinforced sands. Soil Dyn Earthq Eng 181.

Sharo, A.A., Alawneh, A.S., Al Zghool, H.N., Rabab'ah, S.R., 2022. Effect of alkali-resistant glass fibers and cement on the geotechnical properties of highly expansive soil. J Mater Civil Eng 34, 04021417.

Shin, E.C., Das, B.M., Puri, V.K., Yen, S.C., Cook, E.E., 1993. Bearing capacity of strip foundation on geogrid reinforced clay. Geotechnical Testing Journal 16, 534-541.

Shirazi, M.G., Rashid, A.S.A., Nazir, R., Abdul Rashid, A.H., Horpibulsuk, S., 2020. Enhancing the bearing capacity of rigid footing using limited life kenaf geotextile reinforcement. J Nat Fibers 19, 2868-2884.

Sitharam, T.G., Sireesh, S., 2004. Model studies of embedded circular footing on geogrid reinforced sand beds. Ground Improvement 8, 69-75.

Srinivasan, V., Ghosh, P., 2012. Experimental investigation on interaction problem of two nearby circular footings on layered cohesionless soil. Geomechanics and Geoengineering 8, 97-106.

Sukmak, G., 2021. Load bearing capacity of cohesive-frictional soils reinforced with full-wraparound geotextiles: experimental and numerical investigation. Applied Sciences 11, 2973.

Sulaiman, M.S., Mohamad, H.M., Suhaimi, A.A., 2022. A Study on Linear Shrinkage Behavior of Peat Soil Stabilized with Eco-Processed Pozzolan (EPP). Civ Eng J-Tehran 8, 1157-1166.

Susanti, R.D., Waruwu, M., Waruwu, A., 2017. Bearing capacity improvement of peat soil by preloading. ARPN Journal of Engineering and Applied Sciences 12.

Tafreshi, S.M., Shaghaghi, T., Mehrjardi, G.T., Dawson, A.R., Ghadrdan, M., 2015. A simplified method for predicting the settlement of circular footings on multi-layered geocell-reinforced non-cohesive soils. Geotext Geomembranes 43, 332-344.

Talib, F.M., Mohamad, H.M., Mustafa, M.N., 2021. Peat Soil Improvement with Bamboo Reinforcement Technology: A Review. Int J Geomate 21, 75-85.

Tatsuoka, F., Okahara, M., Tanaka, T., Tani, K., Morimoto, T., Siddiquee, M.S.A., 1991. Progressive failure and particle size effect in bearing capacity of a footing on sand, Proc. Geotech. Engrg. Congress. ASCE Geotechnical Special Publication, pp. 788-802.

Terzaghi, K., Peck, R.B., Mesri, G., 1996. Soil mechanics in engineering practice, New York.

Tizpa, P., Chenari, R.J., Payan, M., 2023. PFC/FLAC 3D coupled numerical modeling of shallow foundations seated on reinforced granular fill overlying clay with square void. Comput Geotech 161.

USDA, 1999. Soil taxonomy: A basic system of soil classification for making and interpreting soil surveys, Agriculture handbook, pp. 336-337.

Useche-Infante, D., Aiassa Martínez, G., Arrúa, P., Eberhardt, M., 2023. Scale effect on the behavior of circular footing on geogrid-reinforced sand using numerical analysis. Geomechanics and Geoengineering 18, 34-47.

Useche-Infante, D., Martinez, G.A., Arrua, P., Eberhardt, M., 2022. Experimental study of behaviour of circular footing on geogrid-reinforced sand. Geomech Geoengin 17, 45-63.

Viswanadham, B.V.S., König, D., 2004. Studies on scaling and instrumentation of a geogrid. Geotext Geomembranes 22, 307-328.

Wood, D.M., 2004. Geotechnical modelling. CRC Press.

Wulandari, P.S., Tjandra, D., 2006. Determination of optimum tensile strength of geogrid reinforced embankment, International Civil Engineering Conference towards Sustainable Civil Engineering Practice pp. 187-194.

Yadu, L., Tripathi, R.K., 2013. Effect of the length of geogrid layers in the bearing capacity ratio of geogrid reinforced granular fill-soft subgrade soil system. Procedia - Social and Behavioral Sciences 104, 225-234.

Yaghoobi, B., Fathipour, H., Payan, M., Chenari, R.J., 2023. Bearing capacity of footings on geosynthetic-reinforced soils under combined loading. Geosynth Int, 1-29.

Yalcin, H., Kaya, Z., Çadır, C.C., Uncuoğlu, E., Erol, A., Akin, M., 2023. Improvement of an Undisturbed Peat Soil with Jet Grout Columns: Physical and Numerical Modeling. Arab J Sci Eng 48, 14059-14078.

Yetimoglu, T., Wu, J.T.H., Saglamer, A., 1994. Bearing capacity of rectangular footings on geogrid–reinforced sand. Journal of Geotechnical Engineering 120, 2083-2099.

Yulianto, F.E., Mochtar, N.E., Harwadi, F., 2022. Parameters Changes of Stabilized Fibrous Peat with Environmentally Friendly Materials Due to Water Filtration from the Surroundings on Different of Area Stabilization. Int J Geomate 23, 31-40.

Zuo, Z., Yang, G., Wang, Z., Wang, H., Jin, J., 2021. Effect of boundary conditions on the mechanical behavior of the geogrid–soil interface. Applied Sciences 11, 9942.

ACCEPTED MANUSCRIPT

Zwanenburg, C., Jardine, R.J., 2015. Laboratory, in situ and full-scale load tests to assess flood embankment stability on peat. Geotechnique 65, 309-326.

ACCEPTED MANUSCRIPT

1197 **List of Figures**

1198



(a) (b)

1199 Fig. 1. (a) Visual representation and (b) thickness measurement of peat soil layers from the surface.

1200



(a) (b)

1201 Fig. 2. (a) Excavation to the designated level from the surface and (b) test box installation into peat soil.

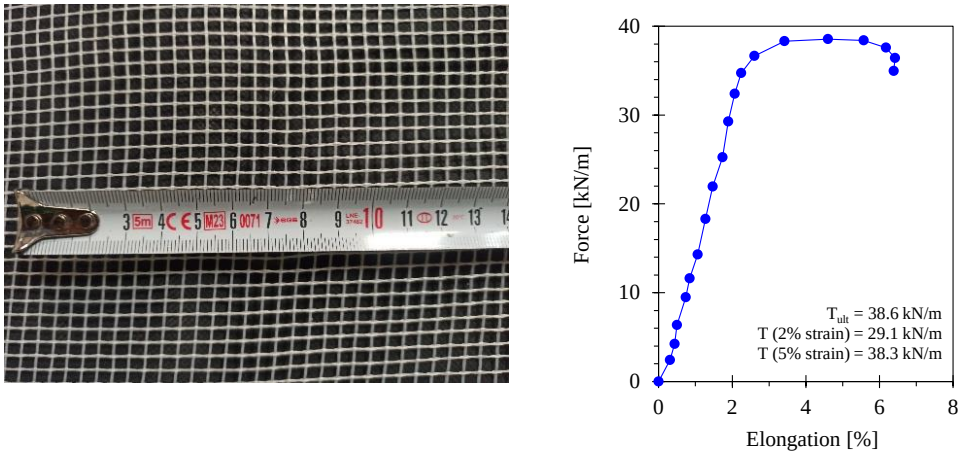
1202



(a1) (a2) (b)

1203 Fig. 3. (a1, a2) Schematic representation of the footing dimensions and (b) application of epoxy adhesive at the footing base.

1204



(a) (b)

Fig. 4. (a) Geogrid with measured aperture size; (b) Corresponding tensile force–elongation curve

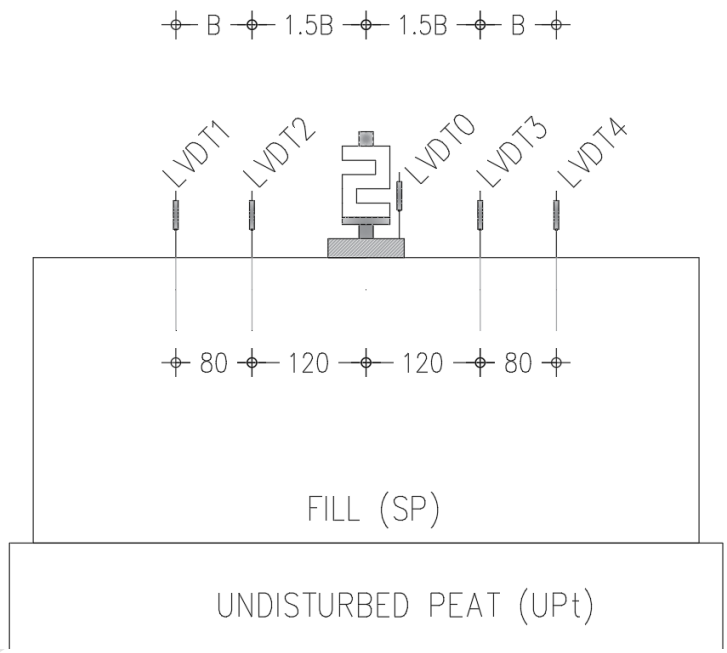


Fig. 5. Test setup with LVDT positioning to measure surface heave.

ACCEPTED MANUSCRIPT

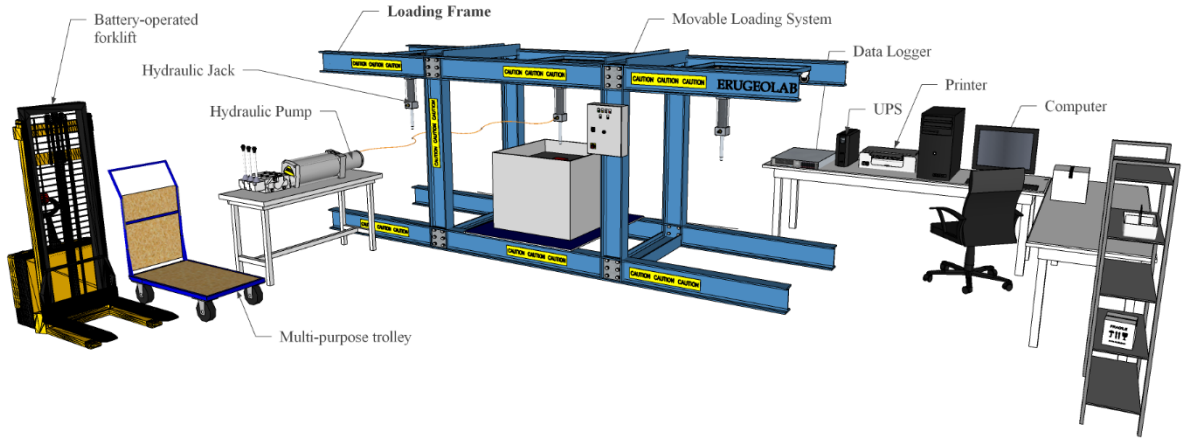


Fig. 6. Schematic of the experimental setup, illustrating the arrangement of the key measurement devices used in the study.

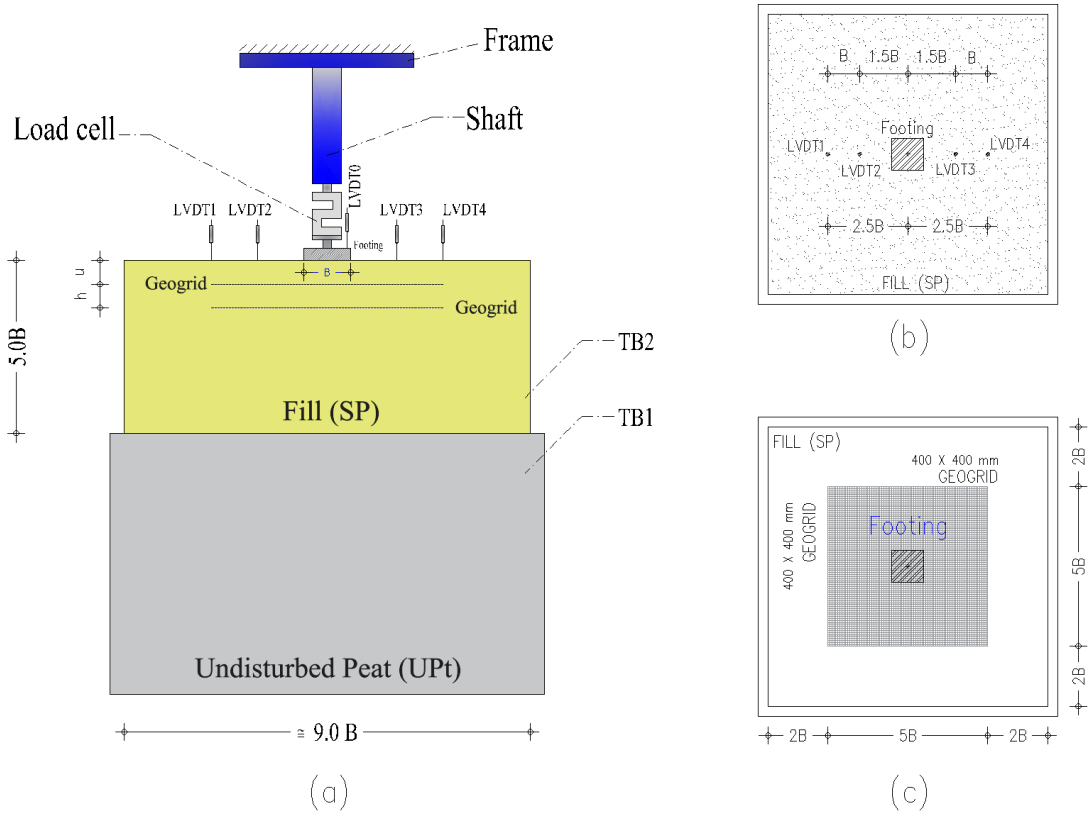


Fig. 7. (a) General test setup, (b) Plan view of LVDT and footing arrangement, (c) Geogrid layout within the fill layer.

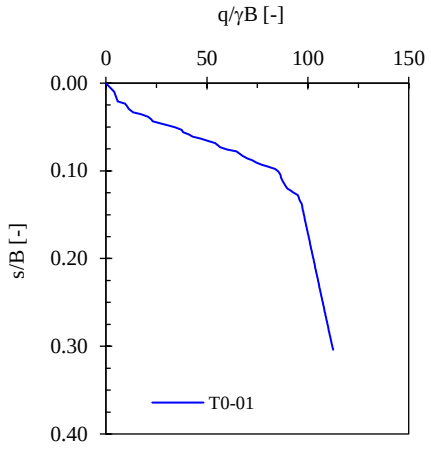


Fig. 8. Loading response of the homogeneous UPt subgrade.

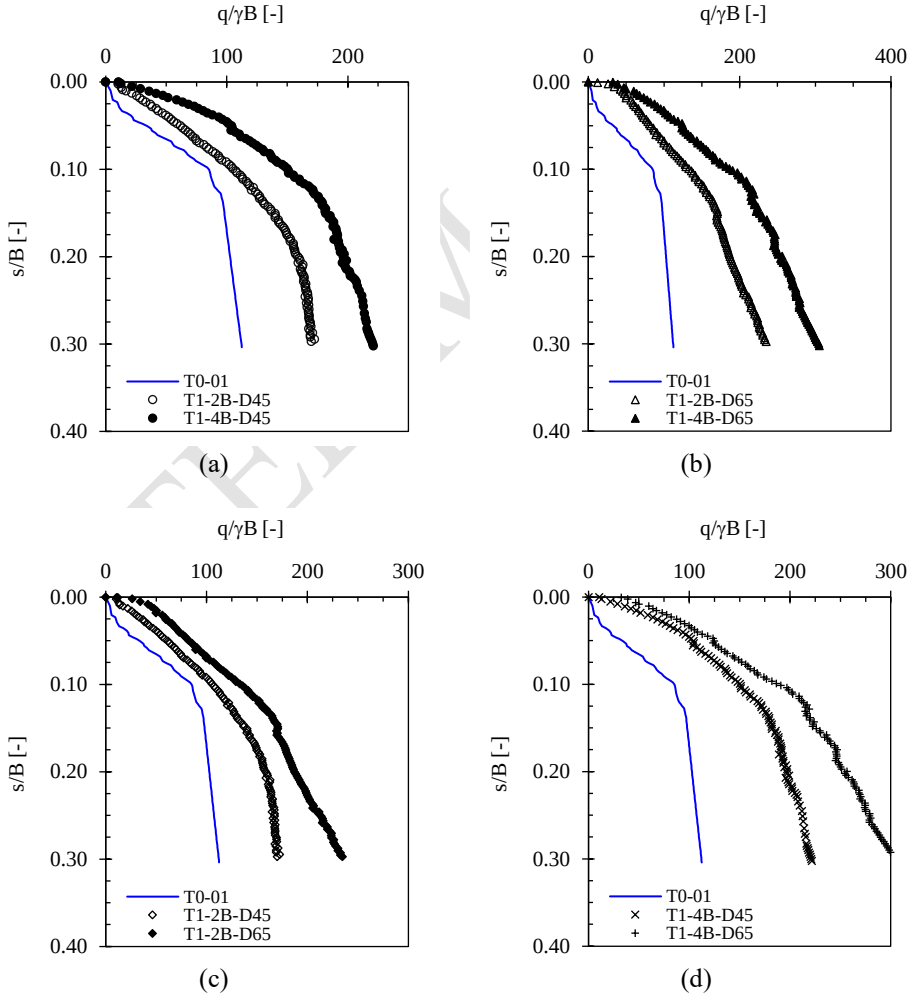


Fig. 9. Effect of H/B ratios at (a) D_r = 45% and (b) D_r = 65%; effect of D_r at (c) H = 2B and (d) H = 4B.

ACCEPTED MANUSCRIPT

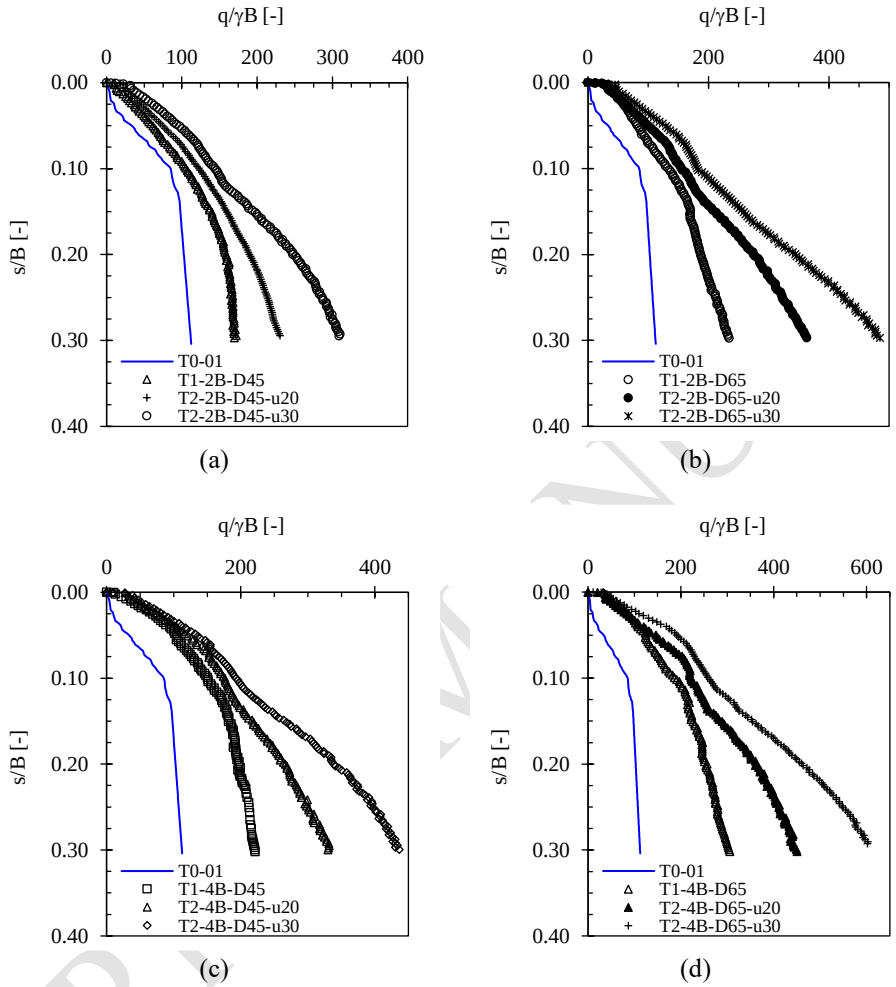


Fig. 10. Effect of u/B ratios for N=1 at: (a) H=2B, D_r = 45%; (b) H=2B, D_r = 65%; (c) H=4B, D_r =45%; and (d) H=4B, D_r =65%.

ACCEPTED MANUSCRIPT

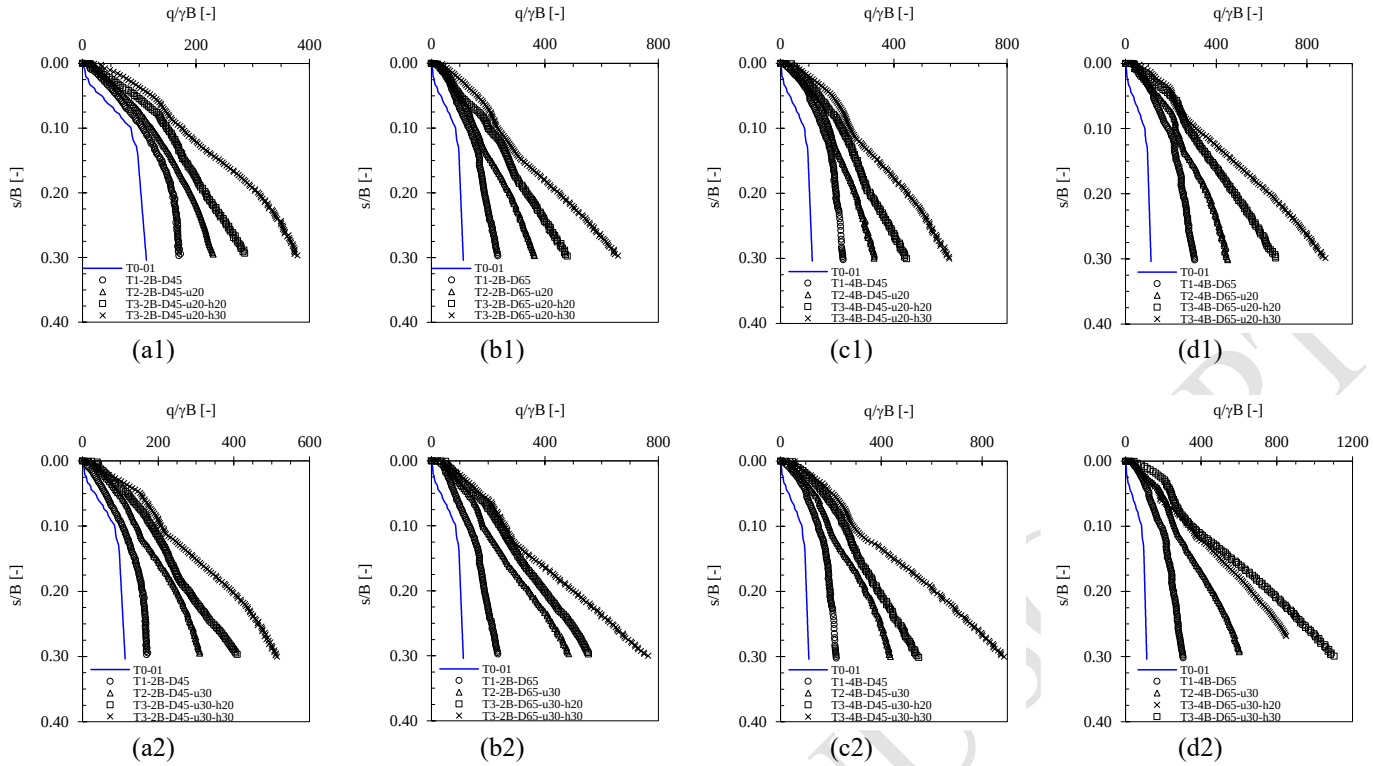


Fig. 11. Effect of h/B ratios on the bearing capacity for various reinforcement configurations: For u = 0.2B: (a1) H=2B, D_r = 45%; (b1) H=2B, D_r = 65%; (c1) H=4B, D_r =45%; (d1) H=4B, D_r =65% (d1). For u = 0.3B: (a2) H=2B, D_r = 45%; (b2) H=2B, D_r = 65%; (c2) H=4B, D_r =45%; (d2) H=4B, D_r =65% (d2).

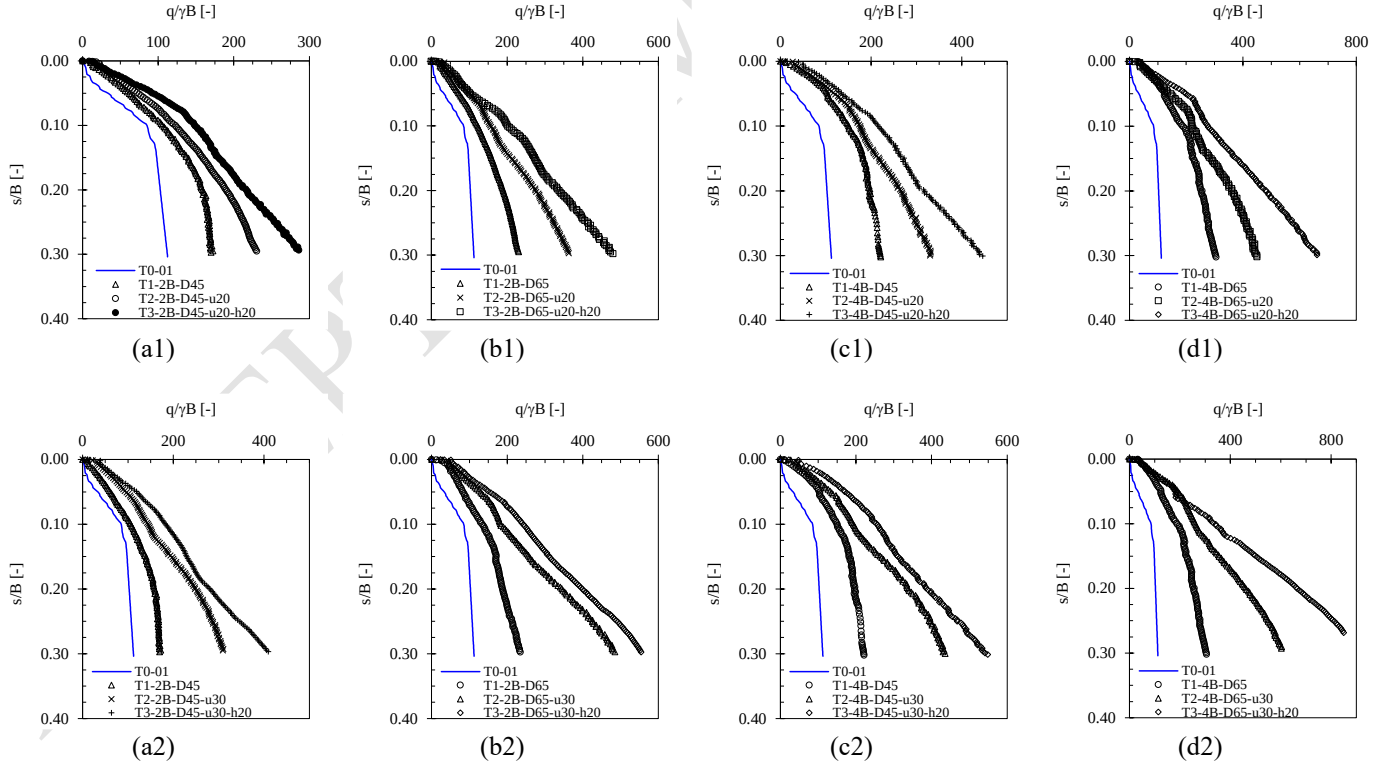
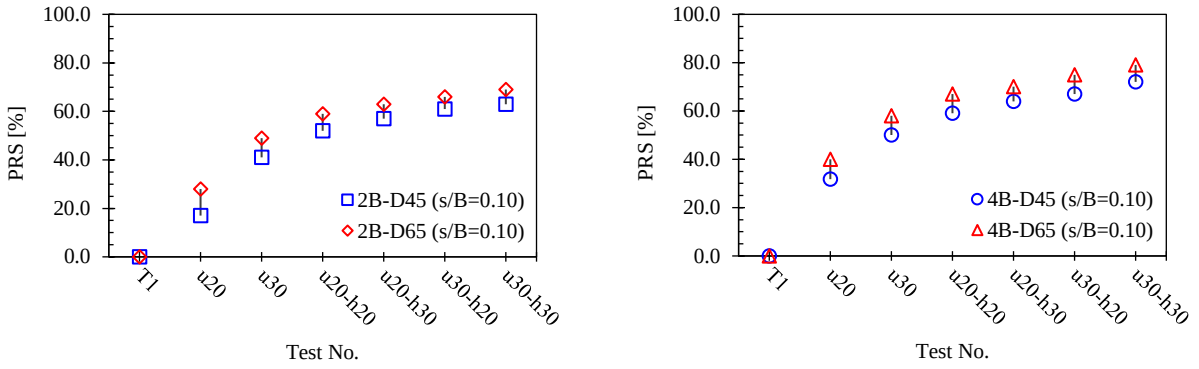
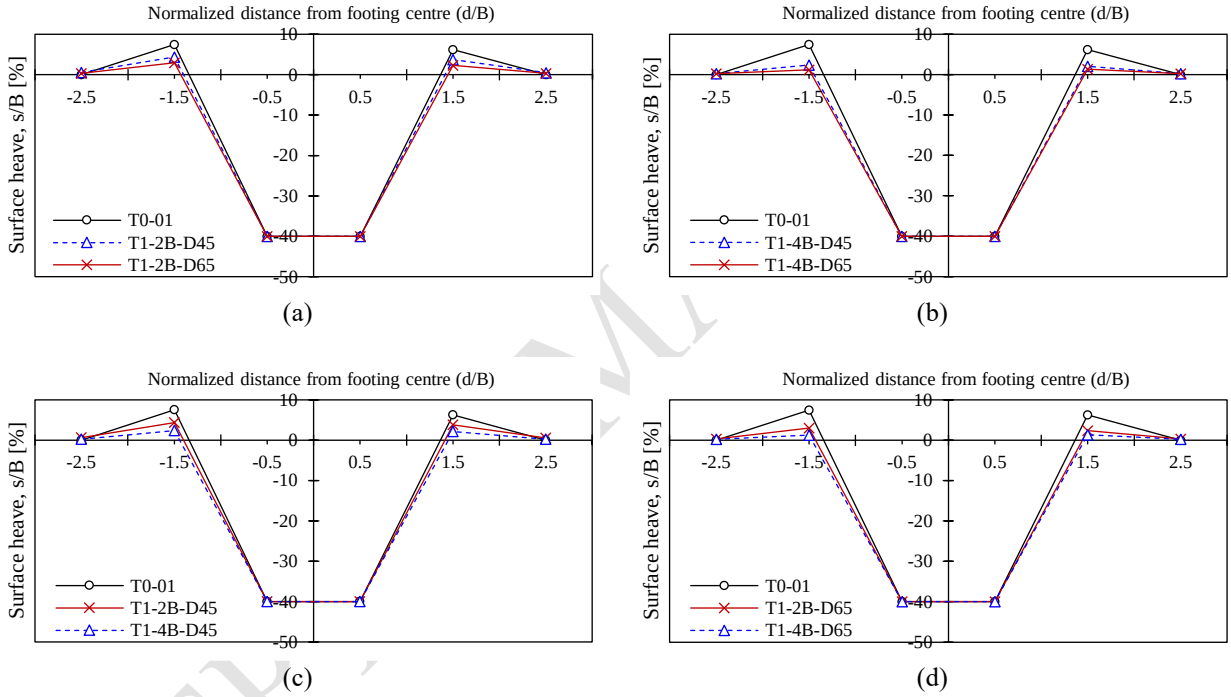


Fig. 12. Effect of reinforcement element number (N=0, 1, and 2) on the bearing capacity of sand fill: For u = 0.2B: (a1) H=2B, D_r = 45%; (b1) H=2B, D_r = 65%; (c1) H=4B, D_r =45%; (d1) H=4B, D_r =65%. For u = 0.3B: (a2) H=2B, D_r = 45%; (b2) H=2B, D_r = 65%; (c2) H=4B, D_r =45%; (d2) H=4B, D_r =65%.



(a) (b)

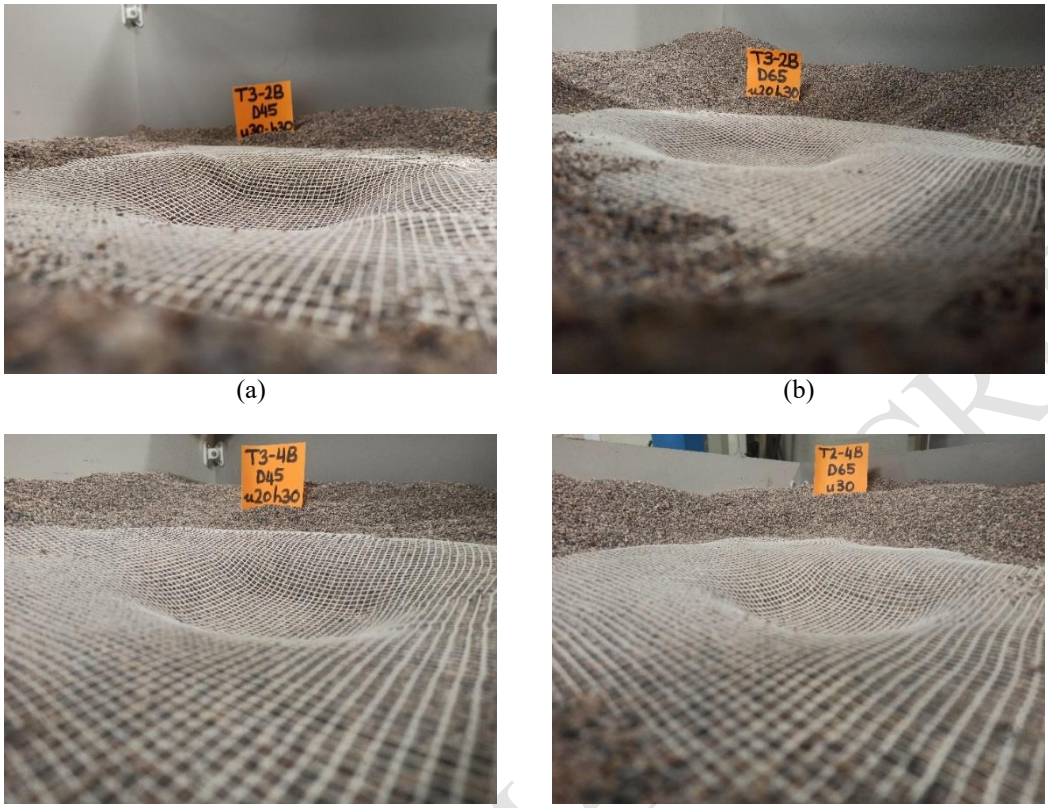
Fig. 13. Comparison of the PRS values for all relative densities for two different H/B ratios: (a) H = 2B and (b) H = 4B.



(a) (b) (c) (d)

Fig. 14. Comparison of the surface heave values for unreinforced tests: (a) H=2B for D_r=45%, (b) H=4B for D_r=65%, (c) D_r=45% for all H/B ratios, and (d) D_r=65% for all H/B ratios.

ACCEPTED MANUSCRIPT



(a) (b)

(c) (d)

Fig. 15. Geogrid deformation for configurations (a) to (d), highlighting the effects of Dr, H/B ratio, and reinforcement layout.

ACCEPTED MANUSCRIPT

List of Tables

Table 1 Mechanical properties of the sand used in the present research.

Tested material	Sand	
Specific gravity	2.66	
Particle size range [mm]	0.85-2.00	
Maximum dry unit weight [kN/m³]	16.68	
Minimum void ratio	0.566	
Minimum dry unit weight [kN/m³]	14.13	
Maximum void ratio	0.847	
D_{10} [mm]	0.94	
D_{30} [mm]	1.13	
D_{50} [mm]	1.18	
D_{60} [mm]	1.29	
Coefficient of curvature	1.05	
Coefficient of uniformity	1.37	
Soil type classification (USCS)	SP	
Relative densities [%]	D_r=45% (1)	D_r=65% (2)
Internal friction angle, ϕ_{tr} [°]	34.2	35.4
Void ratio	0.721	0.664
Dry unit weight [kN/m³]	15.16	15.68

Table 2 Characterization of geotechnical properties and soil classification for peat.

Tested material	Peat
Moisture content [%] (mean)	191.6
Specific gravity	1.87
Unconfined compressive strength [kPa]	19.6
Undrained shear strength [kPa]	9.8
Internal friction angle [°]	29.8
Organic matter content [%]	28.6
pH	8.9
Soil type classification (USCS)	OH
Soil type classification (von Post)	H4-H6

Table 3 Summary of sample quality assessment parameters and criteria from leading studies.

Sample Quality	Andresen and Kolstad	Lunne et al. *for OCR=1-2*	Lunne et al. *for OCR=2-4*	Karlsrud and Hernandez-M.
Criteria	ε_v	$\Delta e/e_0$ and OCR	$\Delta e/e_0$ and OCR	M_0/M_L
Very poor	>10.00	>0.14	>0.10	<1.00
Poor	4.00-10.00	0.07-0.14	0.05-0.10	1.00-1.50
Good to fair	1.00-4.00	0.04-0.07	0.03-0.05	1.50-2.00
Very good to excellent	<1.00	0.03-0.05	<0.03	>2.00
Peat soil in the present research → calculated OCR=1.61-1.90				
Very good to excellent	**0.03-0.71**	**0.008-0.023**	**-**	**1.95-2.87**

**Karlsrud and Hernandez-M.: Karlsrud and Hernandez-Martinez*

ACCEPTED MANUSCRIPT

Table 4 Reinforcement element parameters overview.

Physical characteristics of planar reinforcement (geogrid)	
Parameters	Description
Name	FT 160
Polymer	E-Glass (alkali-resistant glass fibers)
Mass per unit area [g/m²]	160.0
Roll width [mm]	1000
Mesh aperture size [mm]	4.0 x 4.0
Mechanical characteristics of planar reinforcement (geogrid)	
Test type	Wide-width tensile test
Testing protocol	TS EN ISO 10319
Load cell capacity [kN]	50.0
Test rate [%/min]	20.0
Pre-load [kN/m]	0.2
Tensile strength at strain 2% [kN/m]	29.1
Tensile strength at strain 5% [kN/m]	38.3
Tensile strength at strain 8% [kN/m]	38.4
Ultimate tensile strength [kN/m]	38.6
Strain at nominal load [kN/m]	1.4

Table 5 Overview of reduced-scale model tests conducted on geosynthetic-reinforced foundations (Guo et al., 2020).

Researchers	Soil	Reinforcement	Optimum reinforcement parameters					IF_{max}
			N	L	u	h	d_r	
(Guido et al., 1986)	Square	Geogrid	3	3.0B	0.25B	0.25B	0.75B	2.80
(Omar et al., 1993)	Square	Geogrid	-	4.5B	0.40B	-	1.40B	2.00-3.00
(Alawaji, 2001)	Circular	Geogrid	1	4.0D	0.10D	0.10D	0.10D	3.20
(Sitharam and Sireesh, 2004)	Circular	Geogrid	6	6.0D	0.30D	0.40D	2.30D	3.24
(Basudhar et al., 2007)	Circular	Geotextile	3	3.5D	0.25D	1.00D	2.25D	5.50
(Latha and Somwanshi, 2009)	Square	Geogrid	-	4.0B	-	0.40B	2.00B	2.00-2.50
(Abu-Farsakh et al., 2013)	Square	Geogrid	-	6.0B	0.33B	-	1.25B	1.60
(Useche-Infante et al., 2022)	Circular	Geogrid	4-5	3D-5D	0.25-0.40D	0.25D	-	3.15-3.60

D: diameter of the footing and B: width of the footing

Table 6 Test series and parameter configurations.

Test series	Number of tests	Parameters of tests						Description
		Constant	Variable parameters					
			N	H/B	Dr	u/B	h/B	
T0	1	B=80 mm	-	-	-	-	-	Baseline test on peat soil without fill and geogrid reinforcement
T1	4	B=80 mm L/B=5.0	-	2.0 4.0	45% 65%	-	-	Similar to T0, but with fill placed at varying relative densities (D_r) to assess the effect of D_r on bearing capacity and settlement, without geogrid reinforcement.
T2	8	B=80 mm L/B=5.0	1	2.0 4.0	45% 65%	0.20 0.30	-	One geogrid layer placed at varying depths to evaluate reinforcement effects on bearing capacity and settlement.
T3	16	B=80 mm L/B=5.0	2	2.0 4.0	45% 65%	0.20 0.30	0.20 0.30	Two geogrid layers at different depths and spacings to assess reinforcement effects.

ACCEPTED MANUSCRIPT

Table 7 Scaling laws for model test parameters.

Parameters	Scale factor
Mass density	1
Length	$1/\lambda$
Displacement	$1/\lambda$
Tensile strength	$1/\lambda^2$

Table 8 Experimental setup overview: IF codes, test parameters, and associated identifiers.

IF code	Status	Tests identifiers	
IF_0	H=0B, N=0	T0-01	
IF_1	H=2B, D_r=45%, N=0	T1-2B-D45	
	H=2B, D_r=45%, N=1	T2-2B-D45-u20	T2-2B-D45-u30
	H=2B, D_r=45%, N=2	T3-2B-D45-u20-h20 T3-2B-D45-u30-h20	T3-2B-D45-u20-h30 T3-2B-D45-u30-h30
IF_2	H=2B, D_r=65%, N=0	T1-2B-D65	
	H=2B, D_r=65%, N=1	T2-2B-D65-u20	T2-2B-D65-u30
	H=2B, D_r=65%, N=2	T3-2B-D65-u20-h20 T3-2B-D65-u30-h20	T3-2B-D65-u20-h30 T3-2B-D65-u30-h30
IF_3	H=4B, D_r=45%, N=0	T1-4B-D45	
	H=4B, D_r=45%, N=1	T2-4B-D45-u20	T2-4B-D45-u30
	H=4B, D_r=45%, N=2	T3-4B-D45-u20-h20 T3-4B-D45-u30-h20	T3-4B-D45-u20-h30 T3-4B-D45-u30-h30
IF_4	H=4B, D_r=65%, N=0	T1-4B-D65	
	H=4B, D_r=65%, N=1	T2-4B-D65-u20	T2-4B-D65-u30
	H=4B, D_r=65%, N=2	T3-4B-D65-u20-h20 T3-4B-D65-u30-h20	T3-4B-D65-u20-h30 T3-4B-D65-u30-h30

u: first embedment depth, h: vertical distance between two reinforcement layers, D: relative density of fill, H: depth of fill layer

Table 9 Detailed IF code descriptions for all model test scenarios.

IF code	Status	Denotations	Mathematical relation
IF0	H=0B, N=0	q_0: ultimate bearing capacity of the unreinforced UPt q_R: ultimate bearing capacity of the reinforced fill at same settlement	$IF_0 = q_R / q_0$
IF1	H=2B, D_r=45%, N=0 H=2B, D_r=45%, N=1-2	q_{1U}: ultimate bearing capacity of the unreinforced fill q_{1R}: ultimate bearing capacity of the reinforced fill at same settlement	$IF_1 = q_{1R} / q_{1U}$
IF2	H=2B, D_r=65%, N=0 H=2B, D_r=65%, N=1-2	q_{2U}: ultimate bearing capacity of the unreinforced fill q_{2R}: ultimate bearing capacity of the reinforced fill at same settlement	$IF_2 = q_{2R} / q_{2U}$
IF3	H=4B, D_r=45%, N=0 H=4B, D_r=45%, N=1-2	q_{3U}: ultimate bearing capacity of the unreinforced fill q_{3R}: ultimate bearing capacity of the reinforced fill at same settlement	$IF_3 = q_{3R} / q_{3U}$
IF4	H=4B, D_r=65%, N=0 H=4B, D_r=65%, N=1-2	q_{4U}: ultimate bearing capacity of the unreinforced fill q_{4R}: ultimate bearing capacity of the reinforced fill at same settlement	$IF_4 = q_{4R} / q_{4U}$

Note: In this context, the notation "1U" in the term q_{1U} represents the unreinforced condition for Test Series 1, while "1R" in the term q_{1R} denotes the reinforced condition within the same test series. This nomenclature is consistently applied to all consecutive test series presented in the table.

ACCEPTED MANUSCRIPT

Table 10 Summary of ultimate bearing capacity and IF values for the effect of u/B ratios.

Test info	Symbol	Bearing capacity [kPa]	IF_0	IF_1	IF_2	IF_3	IF_4
T0-01	q_0	74.63	1.00	-	-	-	-
T1-2B-D45	q_{1U}	107.66	1.44	1.00	-	-	-
T2-2B-D45-u20	q_{1R}	122.79	1.65	1.14	-	-	-
T2-2B-D45-u30		144.28	1.93	1.34	-	-	-
T1-2B-D65	q_{2U}	135.93	1.82	-	1.00	-	-
T2-2B-D65-u20	q_{2R}	157.46	2.11	-	1.16	-	-
T2-2B-D65-u30		181.72	2.43	-	1.34	-	-
T1-4B-D45	q_{3U}	150.22	2.01	-	-	1.00	-
T2-4B-D45-u20	q_{3R}	176.04	2.36	-	-	1.17	-
T2-4B-D45-u30		192.72	2.58	-	-	1.28	-
T1-4B-D65	q_{4U}	186.36	2.50	-	-	-	1.00
T2-4B-D65-u20	q_{4R}	221.12	2.96	-	-	-	1.19
T2-4B-D65-u30		258.26	3.46	-	-	-	1.39

Table 11 Overview of ultimate bearing capacity and IF values with respect to h/B ratio changes.

Test info	Symbol	Bearing capacity [kPa]	IF_0	IF_1	IF_2	IF_3	IF_4
T0-01	q_0	74.63	1.00	-	-	-	-
T1-2B-D45	q_{1U}	107.66	1.44	1.00	-	-	-
T3-2B-D45-u20-h20	q_{1R}	148.99	2.00	1.38	-	-	-
T3-2B-D45-u20-h30		175.62	2.35	1.63	-	-	-
T3-2B-D45-u30-h20		184.81	2.48	1.72	-	-	-
T3-2B-D45-u30-h30		206.42	2.77	1.92	-	-	-
T1-2B-D65	q_{2U}	135.93	1.82	-	1.00	-	-
T3-2B-D65-u20-h20	q_{2R}	201.96	2.71	-	1.49	-	-
T3-2B-D65-u20-h30		233.62	3.13	-	1.72	-	-
T3-2B-D65-u30-h20		243.63	3.26	-	1.79	-	-
T3-2B-D65-u30-h30		259.56	3.48	-	1.91	-	-
T1-4B-D45	q_{3U}	150.22	2.01	-	-	1.00	-
T3-4B-D45-u20-h20	q_{3R}	214.07	2.87	-	-	1.43	-
T3-4B-D45-u20-h30		243.85	3.27	-	-	1.62	-
T3-4B-D45-u30-h20		256.99	3.44	-	-	1.71	-
T3-4B-D45-u30-h30		289.01	3.87	-	-	1.92	-
T1-4B-D65	q_{4U}	186.36	2.50	-	-	-	1.00
T3-4B-D65-u20-h20	q_{4R}	275.12	3.69	-	-	-	1.48
T3-4B-D65-u20-h30		311.82	4.18	-	-	-	1.67
T3-4B-D65-u30-h20		341.62	4.58	-	-	-	1.83
T3-4B-D65-u30-h30		352.16	4.72	-	-	-	1.89

ACCEPTED MANUSCRIPT

Table 12 Percentage variation in bearing capacity to the number of reinforcement elements.

N	Test info	q [kPa]	q_{differ} [%]	Mean [%]	N	Test info	q [kPa]	q_{differ} [%]	Mean [%]
N=0	T0-01	74.63	-	-					
N=0	T1-2B-D45	107.66	-	-	N=0	T1-4B-D45	150.22	-	-
N=1	T2-2B-D45-u20	122.79	14.1	24.1	N=1	T2-4B-D45-u20	176.04	17.2	22.8
	T2-2B-D45-u30	144.28	34.0			T2-4B-D45-u30	192.72	28.3	
N=2	T3-2B-D45-u20-h20	148.99	38.4	66.2	N=2	T3-4B-D45-u20-h20	214.07	42.5	67.1
	T3-2B-D45-u20-h30	175.62	63.1			T3-4B-D45-u20-h30	243.85	62.3	
	T3-2B-D45-u30-h20	184.81	71.7			T3-4B-D45-u30-h20	256.99	71.1	
	T3-2B-D45-u30-h30	206.42	91.7			T3-4B-D45-u30-h30	289.01	92.4	
N=0	T1-2B-D65	135.93	-	-	N=0	T1-4B-D65	186.36	-	-
N=1	T2-2B-D65-u20	157.46	15.8	24.8	N=1	T2-4B-D65-u20	221.12	18.7	28.7
	T2-2B-D65-u30	181.72	33.7			T2-4B-D65-u30	258.26	38.6	
N=2	T3-2B-D65-u20-h20	201.96	48.6	72.7	N=2	T3-4B-D65-u20-h20	275.12	47.6	71.8
	T3-2B-D65-u20-h30	233.62	71.9			T3-4B-D65-u20-h30	311.82	67.3	
	T3-2B-D65-u30-h20	243.63	79.2			T3-4B-D65-u30-h20	341.62	83.3	
	T3-2B-D65-u30-h30	259.56	91.0			T3-4B-D65-u30-h30	352.16	89.0	

q: ultimate bearing capacity at s/B=0.1; q_{differ}: difference in bearing capacity; Mean: average bearing capacity change for a given value of N.

Table 13 Deformation response of reinforcement elements under different test scenarios.

Test code	H/B [-]		D_r [%]		u/B [-]		h/B [-]		Deformation, s [mm]		DAR* [%]	
	2.0	4.0	45	65	0.20	0.30	0.20	0.30	N1	N2	N1	N2
T2-2B-D45-u20	+		+		+				30.0	-	75.0	-
T2-2B-D45-u30	+		+			+			27.0	-	67.5	-
T3-2B-D45-u20-h20	+		+		+		+		25.0	22.0	62.5	55.0
T3-2B-D45-u20-h30	+		+		+			+	23.0	20.0	57.5	50.0
T3-2B-D45-u30-h20	+		+			+	+		18.0	14.0	45.0	35.0
T3-2B-D45-u30-h30	+		+			+		+	17.0	12.0	42.5	30.0
T2-2B-D65-u20	+			+	+				31.5	-	78.8	-
T2-2B-D65-u30	+			+		+			28.5	-	71.3	-
T3-2B-D65-u20-h20	+			+	+		+		23.0	20.0	57.5	50.0
T3-2B-D65-u20-h30	+			+	+			+	22.0	17.0	55.0	42.5
T3-2B-D65-u30-h20	+			+		+	+		18.0	13.0	45.0	32.5
T3-2B-D65-u30-h30	+			+		+		+	17.0	12.0	42.5	30.0
T2-4B-D45-u20		+	+		+				32.0	-	80.0	-
T2-4B-D45-u30		+	+			+			31.0	-	77.5	-
T3-4B-D45-u20-h20		+	+		+		+		28.0	25.0	70.0	62.5
T3-4B-D45-u20-h30		+	+		+			+	25.0	22.0	62.5	55.0
T3-4B-D45-u30-h20		+	+			+	+		26.0	23.0	65.0	57.5
T3-4B-D45-u30-h30		+	+			+		+	25.0	22.0	62.5	55.0
T2-4B-D65-u20		+		+	+				34.0	-	85.0	-
T2-4B-D65-u30		+		+		+			31.5	-	78.8	-
T3-4B-D65-u20-h20		+		+	+		+		24.0	19.0	60.0	47.5
T3-4B-D65-u20-h30		+		+	+			+	25.0	18.0	62.5	45.0
T3-4B-D65-u30-h20		+		+		+	+		22.0	18.0	55.0	45.0
T3-4B-D65-u30-h30		+		+		+		+	23.0	16.0	57.5	40.0

*DAR: Displacement accommodation ratio

ACCEPTED MANUSCRIPT